Journal of Sound and Vibration 330 (2011) 902–922

Contents lists available at ScienceDirect

Journal of Sound and Vibration

journal homepage: www.elsevier.com/locate/jsvi

Generalized framework for robust design of tuned mass damper systems

Arash Mohtat [a,1], Ehsan Dehghan-Niri [b,*]

[a] School of Mechanical Engineering, University of Tehran, P.O. Box 11155-4563, Tehran, Iran
[b] School of Civil Engineering, University of Tehran, P.O. Box 11155-4563, Tehran, Iran

ARTICLE INFO

Article history:
Received 27 April 2009
Received in revised form
31 August 2010
Accepted 6 September 2010
Handling Editor: D.J. Wagg
Available online 16 October 2010

ABSTRACT

The primary purpose of this contribution is to develop a novel framework for generalized robust design of tuned mass damper (TMD) systems as passive vibration controllers for uncertain structures. This versatile strategy is intended to be free of any restriction on the structure–TMD system configuration, the performance criterion, and the number of uncertain parameters. The main idea pursued is to adopt methods and concepts from the robust control literature, including: (1) the linear fractional transformation (LFT) formulation pertaining to the structured singular value (μ) framework; (2) the concept of weighted multi-input multi-output (MIMO) norms for characterizing performance; and (3) a worst-case performance assessment method to avoid the unacceptable computation burden involved with exhaustive search or Monte Carlo methods in the presence of multiple uncertainties. Based on these, the robust design framework is organized into four steps: (1) modeling and casting the overall dynamics into the proposed LFT framework that isolates the TMD system as the controller, and the uncertainties as a structured perturbation to the nominal dynamics; (2) setting up the optimization problem based on generalized indices of nominal performance, robustness, and worst-case performance; (3) implementing a genetic algorithm (GA) for solution of the optimization problem; and (4) post-processing the results for systematic visualization, validation, and selection of preferred designs. This strategy has been implemented on several illustrative design examples involving a seismically excited multi-story building with different combinations of assumptions on the uncertainty, TMD configuration, excitation scenarios, and performance criteria. The resulting solution sets have been studied through various post-processing methods, including visualization of Pareto fronts, uncertain frequency response plots, time-domain simulations, and random vibration analysis.

1. Introduction

Due to advantages of efficacy, reliability, and low cost, TMD systems have been extensively studied for implementation on various structures, such as buildings [1,2], bridges [3], and tension leg platforms [4]. Some possible TMD realization schemes for controlling horizontal motion of buildings (including spring-damper, rubber bearings, and various pendulum schemes) have been discussed in [5]. Sometimes innovative physical realizations are also possible, e.g. see the roof-garden TMD design

* Corresponding author.
E-mail addresses: amohtat@ut.ac.ir, amohtat@cim.mcgill.ca (A. Mohtat), edehghan@ut.ac.ir, edehghan_niri@yahoo.com (E. Dehghan-Niri).
[1] Current address: Department of Mechanical Engineering and Centre for Intelligent Machines, McGill University, 817 Sherbrooke St. West, Montreal, Quebec, Canada H3A 2K6.

0022-460X/$ - see front matter © 2010 Elsevier Ltd. All rights reserved.
doi:10.1016/j.jsv.2010.09.007

Nomenclature

Important symbols

d disturbance input vector, e.g. ground acceleration and wind loading
e normalized control-target (error) output vector
$\mathbf{F}_c$ control force input to the plant exerted from the TMD system
J_{NP}, J_R, and J_{WCP} indices of nominal performance, robustness, and worst-case performance
$\mathbf{K}(s)$ TMD system as the controller
$\mathbf{P}(s)$ plant dynamics, either 2-in/2-out ports or 3-in/3-out ports
v normalized disturbance input vector
$\mathbf{W}_I(s)$, $\mathbf{W}_O(s)$ input/output weighting filters
y feedback output vector from the plant (input to the controller)
z control-target (error) output vector
δ uncertain real scalar element, $-1 \le \delta \le 1$
$\mathbf{\Delta}$ structured uncertainty perturbation block

Some mathematical notations and definitions

$\left[\begin{array}{c|c} \mathbf{A} & \mathbf{B} \\ \hline \mathbf{C} & \mathbf{D} \end{array}\right]$ shorthand for system transfer matrix $\mathbf{C}(s\mathbf{I}-\mathbf{A})^{-1}\mathbf{B}+\mathbf{D}$, corresponding to the state-space realization:
$\dot{\mathbf{x}} = \mathbf{A}\mathbf{x}+\mathbf{B}\mathbf{v}$
$\mathbf{y} = \mathbf{C}\mathbf{x}+\mathbf{D}\mathbf{v}$

lower and upper LFTs defined as (provided that the matrix inverses exist):
$\mathcal{F}_\ell(\mathbf{M},\mathbf{N})$ $\mathcal{F}_\ell(\mathbf{M},\mathbf{N}) = \mathbf{M}_{11}+\mathbf{M}_{12}\mathbf{N}(\mathbf{I}-\mathbf{M}_{22}\mathbf{N})^{-1}\mathbf{M}_{21}$
$\mathcal{F}_u(\mathbf{M},\mathbf{Q})$ $\mathcal{F}_u(\mathbf{M},\mathbf{Q}) = \mathbf{M}_{22}+\mathbf{M}_{21}\mathbf{Q}(\mathbf{I}-\mathbf{M}_{11}\mathbf{Q})^{-1}\mathbf{M}_{12}$
where $\mathbf{N} \in \mathbb{C}^{q_2\times p_2}$, $\mathbf{Q} \in \mathbb{C}^{q_1\times p_1}$ and $\mathbf{M} \in \mathbb{C}^{(p_1+p_2)\times(q_1+q_2)}$ is consistently partitioned

List of acronyms

DMF dynamic magnification factor
FRF frequency response function
GA genetic algorithm
LFT linear fractional transformation
LMI linear matrix inequality
MIMO multi-input multi-output
SDOF single degree of freedom
SISO single-input single-output
SSV structured singular value (μ)
TITO two-port input, two-port output
TMD (also: STMD, MTMD, UMTMD, IMTMD) tuned mass damper, also: single TMD, multiple TMD (MTMD), uniform MTMD, irregular MTMD

in the aforementioned reference. From a theoretical point of view, on the other hand, the STMD can be regarded as a narrow-band filter tuned to the first structural frequency. This leads to vulnerability to mistuning effects [6] and degradation of the STMD efficacy in mitigating structural response against excitations with a wide spectrum of frequency contents, like seismic loads [2]. Moreover, a single massive TMD is rather difficult to install and maintain [7]; and, when subjected to dynamic impulsive loads (like earthquake excitations) filtered through the structure, does not reach its full energy-absorbing potential as quickly as required [2]. These factors have motivated the application of systems with several TMD units covering a frequency range and/or physically distributed in space. In this paper, the term "TMD system" refers to any such configuration of a number of TMD units installed on a generic structure. Examples of these configurations include the dual TMD [8] also referred to as bi-TMD [9]; double TMD [10]; double-layered TMD [10]; interconnected multiple TMD [11] (interconnection of TMDs in series); and, non-interconnected MTMD (NI-MTMD) [11] or simply referred to as MTMD which is the most broadly used configuration. Different assumptions on the parameters have been considered for design of TMD systems. For instance, in the MTMD case, equal masses and damping ratios along with uniform distribution of frequency ratios can be assumed for the TMD units to simplify the design; resulting in a uniform MTMD (UMTMD) [12] compared to the irregular MTMD (IMTMD) [13] where frequency and damping ratios of the TMD units constitute individual design variables. As previously pointed out, some other investigations study physical distribution of TMD devices on structures, e.g. references [1,2] study optimal placement of TMDs on building floors. Despite this extensive research, there is almost no study that offers a convenient method and formulation to accommodate any arbitrary combination of structure–TMD system within a unified approach. Other limitations of the investigations available in the literature are discussed in what follows.

In practice, structures and their dynamic characteristics are subjected to uncertainties in the mass, damping and stiffness originating from a variety of sources, such as inadequate modeling of the boundary conditions at the structural joints, effects of nonstructural elements, degradation due to aging, and fluctuations in structural mass, as well as uncertainties in the member capacities, yield strengths, etc. Furthermore, the dynamic characteristics of structures change under earthquake or wind excitations. Some structures have uncertain nonlinear properties even in the small amplitude range due to the contribution of secondary members [15,16]. Therefore, in practical design problems, robustness of the TMD system to uncertainties must be treated as a design concern to avoid undesired performance degradation and mistuning effects. Nevertheless, in most of the previous works, optimization of the TMD systems was based on effectiveness; and, robustness was either not considered [17–21] or qualitatively checked and commented on, only after the design [7,12,22–25]. See the brief discussion in [16] with further details on these studies and the qualitative concepts regarding robustness. However, quite recently more attention has been dedicated to the issue of robustness in TMD systems. Hoang and Warnitchai [26] proposed a robustness index defined as an average performance of several samples of the uncertain system with the uncertain parameters following a specified

probability distribution. Their procedure, although rather extendable to situations more general than MTMDs for SDOF structures (the numerical example considered in that paper), is limited to mean square structural response reduction against stationary stochastic excitation due to the Lyapunov-based formulation of the performance function and its gradient. In another case in point, Li and Ni [27] proposed a rigorous gradient-based method that has the ability to design a robustly effective IMTMD considering a desired level of estimation error in structural parameters. However, this procedure was intended only for minimization of the maximum DMF of structural response (SISO case of H_∞ optimization) and was presented only for a SDOF structure with MTMD. In another relevant research, Dehghan-Niri et al. [16,28] proposed the novel idea of utilizing an index of robustness along with effectiveness within a two-objective evolutionary optimization and demonstrated the efficacy of this methodology for design of uniform and irregular MTMD systems for SDOF main structures with uncertain natural frequency. Similar two-objective GA design methodologies have been proposed in [9,29]. In Ref. [29], Marano et al. proposed the minimization of the mean and standard deviation of the structural displacement covariance computed through sampling as the two objectives. This method aimed only at vibration mitigation of SDOF main systems with STMD against random base acceleration modeled by a stationary filtered white noise process. In Ref. [9], Ok et al. demonstrated the application of GA with nominal and worst-case robust performance indices as the two objectives for design of bi-tuned mass dampers attached to the SDOF main system with uncertain stiffness. The main purpose of the aforementioned investigation was to develop practical optimal design formulae for bi-TMDs within methodology and formulations that maintain simplicity.

In conclusion, each of the available methodologies for design of TMD systems targets a specific purpose and has its own limitations and restrictive assumptions. These limitations can be categorized as:

1) Restrictions on the structure and TMD system configuration, e.g. analytical formulations assuming a SDOF structure with a MTMD.
2) Restriction on design or performance criteria, e.g. a specific SISO norm from a specific excitation to a specific target output.
3) Considering only a simplistic single-parameter uncertainty, or treating the multiple-parameter uncertainty by inefficient Monte Carlo-like (sampling) methods. There exist only few studies that use more computationally efficient asymptotic expansion methods for reliability integrals (e.g. see Ref. [15]). Furthermore, these investigations target only aleatory (stochastic) uncertainties (see Section 4 for a categorization of uncertainty types), and are constrained by conditions to maintain the required analytical formulations tractable.

The present paper, on the other hand, is intended to overcome all these limitations. The first one is handled by the lower LFT formulation introduced in Section 2; the second is resolved via the concept of weighted MIMO norms from any group of disturbance **v** to error outputs **e**; and, the third is tackled through explicit representation of the multiple uncertainties as a structured perturbation block within the rigorous LFT formulation of Section 4.2. This section exploits the SSV (μ) framework [14] and the LFT-based worst-case performance assessment methods [30] in the robust control literature. To facilitate the design of the TMD systems in such a generalized sense, all the concepts, formulations and procedures are collected into the four-step framework shown in Fig. 1.

It should be pointed out that the organization of the paper is not based on the four steps of the framework, but on the logical flow of the concepts. The complete development of the LFT formulation required in Step I is postponed to Section 4.2 after its initial development in Section 2. The procedures associated with Step II are discussed in Sections 3 and 4, while Step

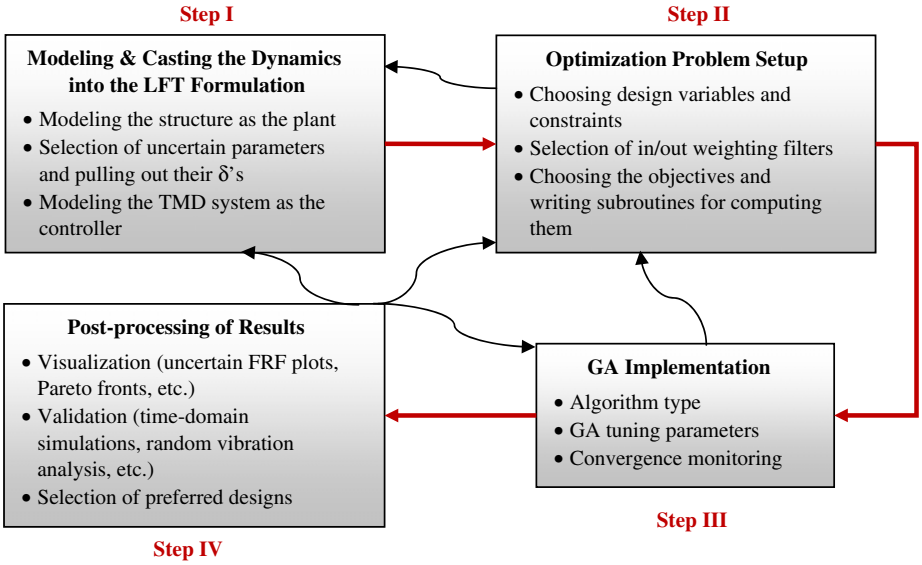

Fig. 1. Flowchart of the proposed framework for robust design of TMD systems.

IV is practically illustrated throughout the examples worked out in Section 5. GA (Step III), on the other hand, is considered a standard optimization tool; hence, there is no specific section dedicated to it. Of course, some important relevant concepts are briefly discussed in Sections 3–5, because the proposed framework greatly owes its simplicity and flexibility to GA.

2. LFT formulation for the structure–TMD system

In this section, we shall show that the dynamics of the structure with the TMD system can be cast as the LFT interconnection of a TITO plant and a feedback controller, as shown in Fig. 2.

Considering disturbance $\mathbf{d}$ and control $\mathbf{F}_c$ as the two groups of inputs, and error output $\mathbf{z}$ and feedback $\mathbf{y}$ as the groups of outputs, the TITO model for the structure referred to in Fig. 2 is

$$\mathbf{P}(s)=\left[\begin{array}{c|cc}\mathbf{A} & \mathbf{B}_d & \mathbf{B}_F \\ \hline \mathbf{C}_z & \mathbf{D}_{zd} & \mathbf{D}_{zF} \\ \mathbf{C}_y & \mathbf{D}_{yd} & \mathbf{D}_{yF}\end{array}\right] \tag{1}$$

while the TMD system model is

$$\mathbf{K}(s)=\left[\begin{array}{c|c}\mathbf{A}_K & \mathbf{B}_K \\ \hline \mathbf{C}_K & \mathbf{D}_K\end{array}\right] \tag{2}$$

and the lower LFT [14] interconnection describing the mapping from the input group of signals $\mathbf{d}$ to the output group $\mathbf{z}$ would be

$$\mathbf{T}_{zd}(s)=\mathcal{F}_\ell(\mathbf{P},\mathbf{K})=\mathbf{P}_{zd}+\mathbf{P}_{zF}\mathbf{K}(\mathbf{I}-\mathbf{P}_{yF}\mathbf{K})^{-1}\mathbf{P}_{yd} \tag{3-I}$$

where

$$\mathbf{P}_{zd}(s)=\left[\begin{array}{c|c}\mathbf{A} & \mathbf{B}_d \\ \hline \mathbf{C}_z & \mathbf{D}_{zd}\end{array}\right],\quad \mathbf{P}_{zF}(s)=\left[\begin{array}{c|c}\mathbf{A} & \mathbf{B}_F \\ \hline \mathbf{C}_z & \mathbf{D}_{zF}\end{array}\right]$$

$$\mathbf{P}_{yd}(s)=\left[\begin{array}{c|c}\mathbf{A} & \mathbf{B}_d \\ \hline \mathbf{C}_y & \mathbf{D}_{yd}\end{array}\right],\quad \mathbf{P}_{yF}(s)=\left[\begin{array}{c|c}\mathbf{A} & \mathbf{B}_F \\ \hline \mathbf{C}_y & \mathbf{D}_{yF}\end{array}\right]$$

are the partitions of the transfer matrix $\mathbf{P}$, consistent with the input/output grouping; or, equivalently:

$$\mathbf{T}_{zd}(s)=\mathcal{F}_\ell(\mathbf{P},\mathbf{K})=\left[\begin{array}{c|c}\mathbf{A}_{CL} & \mathbf{B}_{CL} \\ \hline \mathbf{C}_{CL} & \mathbf{D}_{CL}\end{array}\right] \tag{3-II}$$

where $\mathbf{A}_{CL}$, $\mathbf{B}_{CL}$, $\mathbf{C}_{CL}$, and $\mathbf{D}_{CL}$ are the state-space matrices of the closed-loop system, defined as

$$\mathbf{A}_{CL}=\begin{bmatrix}\mathbf{A}+\mathbf{B}_F\tilde{\mathbf{R}}^{-1}\mathbf{D}_K\mathbf{C}_y & \mathbf{B}_F\tilde{\mathbf{R}}^{-1}\mathbf{C}_K \\ \mathbf{B}_K\mathbf{R}^{-1}\mathbf{C}_y & \mathbf{A}_K+\mathbf{B}_K\mathbf{R}^{-1}\mathbf{C}_{yF}\mathbf{C}_K\end{bmatrix}$$

$$\mathbf{B}_{CL}=\begin{bmatrix}\mathbf{B}_d+\mathbf{B}_F\tilde{\mathbf{R}}^{-1}\mathbf{D}_K\mathbf{C}_{yd} \\ \mathbf{B}_K\mathbf{R}^{-1}\mathbf{C}_{yd}\end{bmatrix}$$

$$\mathbf{C}_{CL}=\begin{bmatrix}\mathbf{C}_z+\mathbf{C}_{zF}\mathbf{D}_K\mathbf{R}^{-1}\mathbf{C}_y & \mathbf{C}_{zF}\tilde{\mathbf{R}}^{-1}\mathbf{C}_K\end{bmatrix}$$

$$\mathbf{D}_{CL}=\mathbf{D}_{zd}+\mathbf{D}_{zF}\mathbf{D}_K\mathbf{R}^{-1}\mathbf{D}_{yd}$$

with $\mathbf{R}=\mathbf{I}-\mathbf{C}_{yF}\mathbf{D}_K$, $\tilde{\mathbf{R}}=\mathbf{I}-\mathbf{D}_K\mathbf{C}_{yF}$.

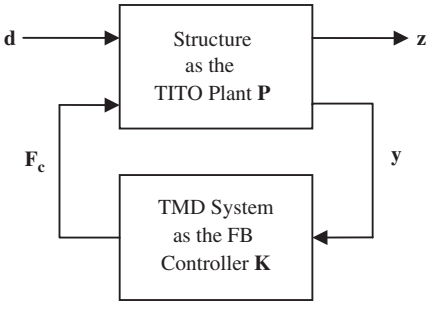

Fig. 2. LFT interconnection of the structural plant and the TMD controller.

This formulation isolates the dynamics of the TMD system to be designed from that of the structural plant, facilitating the performance evaluation of designs. It offers a systematic convenient way for definition of weighted MIMO norms as a means of characterizing the performance of the controlled structural response from disturbance inputs to target quantities (see Section 3). The LFT machinery will be further exploited in Section 4.2 to pull out the parametric uncertainties embedded in the system.

2.1. TITO formulation for the structure

A generic scenario of an N-story shear building subjected to base acceleration and force excitation, as shown in Fig. 3, is utilized to illustrate the required formulation for the structure.

The matrix equation of motion for the structure is as follows:

$$\begin{aligned} \mathbf{M}_s\ddot{\mathbf{u}}+\mathbf{C}_s\dot{\mathbf{u}}+\mathbf{K}_s\mathbf{u} &= -\mathbf{M}_s\mathbf{r}_g a_g+\mathbf{F}_d+\mathbf{F}_{\text{ctrl}} \\ \mathbf{z}_1 &= \mathbf{W}_u\mathbf{u}, \quad \mathbf{z}_2=\ddot{\mathbf{u}}+a_g \end{aligned} \tag{4}$$

where

$\mathbf{M}_s=\text{diag}(m_1, m_2, \ldots, m_N)$ is the structural mass matrix:

$$\mathbf{K}_s=\begin{bmatrix} k_1+k_2 & -k_2 & & & 0 \\ -k_2 & k_2+k_3 & -k_3 & & \\ & & \ddots & & \\ & & -k_{N-1} & k_{N-1}+k_N & -k_N \\ 0 & & & -k_N & k_N \end{bmatrix}$$

is the structural stiffness matrix.

$\mathbf{C}_s=\frac{2\zeta_s\omega_1\omega_2}{\omega_1+\omega_2}\mathbf{M}_s+\frac{2\zeta_s}{\omega_1+\omega_2}\mathbf{K}_s$ is the proportional damping matrix (any other dissipation matrix can be also considered without additional effort, if required) defined based on the damping ratio ζ_s and the first two natural frequencies ω_1, ω_2 of the structure. Note that the dissipation matrix assuming that damping forces depend only on generalized velocities is not the only linear model of vibration damping (see Ref. [31] for a detailed discussion). However, for simplification of the illustration, a dissipation matrix damping is assumed for the shear building model (this does not affect the generality of the framework, because the performance measures are formulated using the plant $\mathbf{P}$ without any assumptions rather than linearity).

$\mathbf{r}_g=[1\ldots1]^{\text{T}}$ is the influence vector of the ground acceleration a_g.

$\mathbf{F}_d$, $\mathbf{F}_{\text{ctrl}}$ are the disturbance forces (e.g. from wind load) and control forces (exerted by the TMD system) to the floors of the building.

$\mathbf{W}_u=\begin{bmatrix} 1 & & & 0 \\ -1 & 1 & & \\ & & \ddots & \\ 0 & & -1 & 1 \end{bmatrix}$ is the weighting matrix utilized to extract the inter-story drifts (floors displacement relative to each other) $\mathbf{z}_1=[u_1, u_2-u_1, \ldots, u_N-u_{N-1}]^{\text{T}}$ out of the floor displacements $\mathbf{u}$ relative to the base

and

$\mathbf{z}_2$ is the vector of floors absolute accelerations.

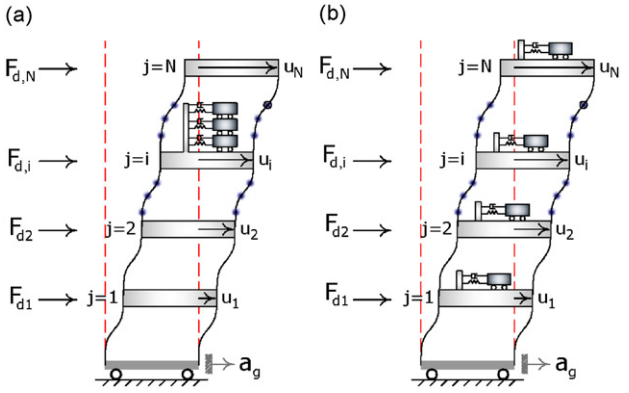

Fig. 3. N-story shear building subjected to base acceleration and force disturbances, equipped with "MTMD on ith floor" (a) and "STMD on every floor" (b) systems.

Now, considering the following definition for the state vector and the input–output groups of the TITO model:

$$\text{states}: \ \mathbf{x}=\begin{Bmatrix}\mathbf{u}\\ \dot{\mathbf{u}}\end{Bmatrix}; \quad \text{inputs}: \ \mathbf{d}=\begin{Bmatrix}a_g\\ \mathbf{F}_d\end{Bmatrix}, \ \mathbf{F}_c=\mathbf{F}_{\text{ctrl}}; \quad \text{outputs}: \ \mathbf{z}=\begin{Bmatrix}\mathbf{z}_1\\ \mathbf{z}_2\end{Bmatrix}, \ \mathbf{y}=\mathbf{z}_2$$

the following definition for the state-space matrices previously used in Eq. (1) would result:

$$\begin{gathered}\mathbf{A}=\begin{bmatrix}\mathbf{0}_{N\times N} & \mathbf{I}_{N\times N}\\ -\mathbf{M}_s^{-1}\mathbf{K}_s & -\mathbf{M}_s^{-1}\mathbf{C}_s\end{bmatrix}, \quad \mathbf{B}_d=\begin{bmatrix}\mathbf{0}_{N\times 1} & \mathbf{0}_{N\times N}\\ -\mathbf{r}_g & \mathbf{M}_s^{-1}\end{bmatrix}, \quad \mathbf{B}_F=\begin{bmatrix}\mathbf{0}_{N\times N}\\ \mathbf{M}_s^{-1}\end{bmatrix}\\ \mathbf{C}_z=\begin{bmatrix}\mathbf{W}_u & \mathbf{0}_{N\times N}\\ -\mathbf{M}_s^{-1}\mathbf{K}_s & -\mathbf{M}_s^{-1}\mathbf{C}_s\end{bmatrix}, \quad \mathbf{D}_{zd}=\begin{bmatrix}\mathbf{0}_{N\times 1} & \mathbf{0}_{N\times N}\\ \mathbf{0}_{N\times 1} & \mathbf{M}_s^{-1}\end{bmatrix}, \quad \mathbf{D}_{zF}=\begin{bmatrix}\mathbf{0}_{N\times N}\\ \mathbf{M}_s^{-1}\end{bmatrix}\\ \mathbf{C}_y=\begin{bmatrix}-\mathbf{M}_s^{-1}\mathbf{K}_s & -\mathbf{M}_s^{-1}\mathbf{C}_s\end{bmatrix}, \quad \mathbf{D}_{yd}=\begin{bmatrix}\mathbf{0}_{N\times 1} & \mathbf{M}_s^{-1}\end{bmatrix}, \quad \mathbf{D}_{yF}=[\mathbf{M}_s^{-1}]\end{gathered} \tag{5}$$

which completely determine the system **P** from disturbance **d** (base acceleration and force excitation) and control $\mathbf{F}_c$ input (TMD system forces exerted to the floors) to error output **z** (inter-story drifts and floors absolute acceleration) and feedback output **y** (absolute acceleration of building floors).

2.2. TMD system as the feedback controller

The equation of motion for a single TMD unit in terms of u_T, its displacement relative to the ground, can be easily derived as

$$m_T(\ddot{u}_T+a_g)=m_T(\ddot{u}_T-\ddot{u}_i+a_i)=-k_T(u_T-u_i)-c_T(\dot{u}_T-\dot{u}_i) \tag{6}$$

where m_T, k_T, and c_T are the TMD mass, stiffness, and damping constant; u_i is the displacement of the TMD support (the ith floor to which the TMD is attached) relative to the ground; and, a_i is the absolute acceleration of the ith floor ($a_i=a_g+\ddot{u}_i$). The right hand side of this equation is the sum of the spring and dashpot force to the TMD mass, the opposite of which is exerted to the TMD support (ith floor) and is denoted by F_i. Therefore, the TMD unit can be regarded as a system block from the support acceleration input (a_i) to the force output (F_i), described by

$$\begin{gathered}\dot{\mathbf{x}}_T=\mathbf{A}_T\mathbf{x}_T+\mathbf{B}_T a_i; \quad \mathbf{x}_T=\begin{bmatrix}u_T-u_i & \dot{u}_T-\dot{u}_i\end{bmatrix}^{\mathrm{T}}\\ F_i=\mathbf{C}_T\mathbf{x}_T\end{gathered} \tag{7}$$

where

$$\mathbf{A}_T=\begin{bmatrix}0 & 1\\ -k_T/m_T & -c_T/m_T\end{bmatrix}, \quad \mathbf{B}_T=\begin{bmatrix}0\\ -1\end{bmatrix}, \quad \mathbf{C}_T=\begin{bmatrix}k_T & c_T\end{bmatrix}$$

Accordingly, each of the TMD systems configurations shown in Fig. 3 (as well as any other possible) can be viewed as an interconnection of single TMD blocks as shown in Fig. 4. From the block-diagram representation of Fig. 4, it can be easily concluded that the state-space matrices of the TMD system as the feedback controller **K** in Eq. (2), for the n-MTMD installed on the ith floor case can be written as

$$[\mathbf{A}_K]_{2n\times 2n}=blkdiag(\mathbf{A}_{T1},\mathbf{A}_{T2},\ldots,\mathbf{A}_{Tn})$$

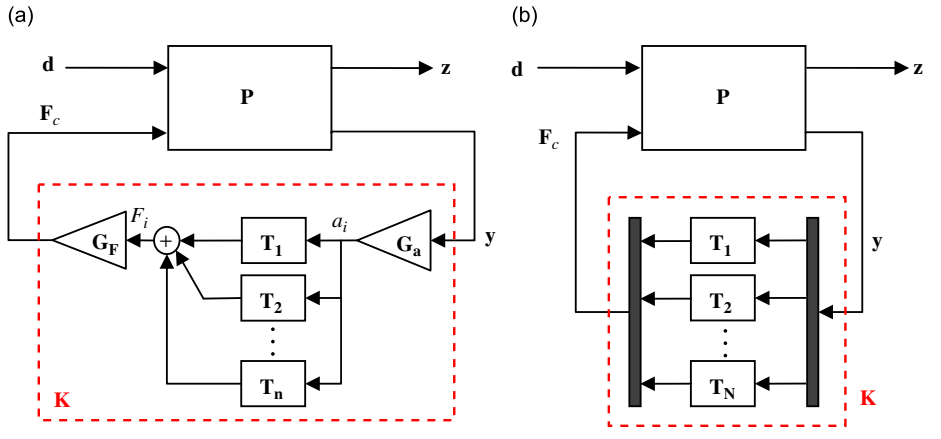

Fig. 4. (a) MTMD interconnection and (b) "STMD on every floor" interconnection.

$$[\mathbf{B}_K]_{2n\times N}=\begin{bmatrix}\mathbf{B}_{T1}\\ \mathbf{B}_{T2}\\ \vdots\\ \mathbf{B}_{Tn}\end{bmatrix}\mathbf{G}_a;\quad \mathbf{G}_a=[g_a(j)]_{1\times N},\quad g_a(j)=\begin{cases}1, & j=i\\ 0 & otherwise\end{cases}$$
$$[\mathbf{C}_K]_{N\times 2n}=\mathbf{G}_F\begin{bmatrix}\mathbf{C}_{T1} & \mathbf{C}_{T2} & \dots & \mathbf{C}_{Tn}\end{bmatrix};\quad \mathbf{G}_F=\mathbf{G}_a^{\mathrm{T}}$$
$$[\mathbf{D}_K]_{N\times N}=\mathbf{0}_{N\times N} \tag{8}$$

where blkdiag refers to the block diagonal arrangement of matrices. On the other hand, for the "STMD on every floor" configuration in Fig. 4b we would have

$$\begin{aligned}[\mathbf{A}_K]_{2n\times 2n}&=\mathrm{blkdiag}(\mathbf{A}_{T1},\mathbf{A}_{T2},\dots,\mathbf{A}_{Tn})\\ [\mathbf{B}_K]_{2n\times N}&=\mathrm{blkdiag}(\mathbf{B}_{T1},\mathbf{B}_{T2},\dots,\mathbf{B}_{Tn})\\ [\mathbf{C}_K]_{N\times 2n}&=\mathrm{blkdiag}(\mathbf{C}_{T1},\mathbf{C}_{T2},\dots,\mathbf{C}_{Tn})\\ [\mathbf{D}_K]_{N\times N}&=\mathbf{0}_{N\times N}\end{aligned} \tag{9}$$

Note that n refers to the number of TMD units, while N is the number of building floors; and, these two coincide in the case of "STMD on every floor". Any other distribution of TMD units on a building can be also formulated in a similar manner. This approach also facilitates the redundancy study of the TMDs (effect of failure of individual TMD units on the overall performance).

3. The nominal performance optimization problem

In the previous section it was shown that in view of the LFT formulation, we can consider the TMD system as a controller for the structure that is intended to improve the closed-loop system response to disturbances. Consequently, a natural performance objective for designing this controller would be reducing the closed-loop gain from disturbance excitations **d** to target outputs **z**. System norms provide a precise measure for this purpose. For a MIMO system, as is the case in point, a weighted matrix system norm would be preferred to account for: (1) relative magnitude of different disturbance signals composing **d**; (2) frequency/spectral content of the signals; and (3) relative importance of error outputs **z** in the design. The input–output weighted configuration for this purpose is shown in Fig. 5.

Accordingly, minimization of the following generalized weighted nominal performance index would be an appropriate criterion for tuning the TMD system design variables **x** to achieve optimal nominal performance:

$$\min_{\mathbf{x}} J_{\mathrm{NP}}=\left\|\mathbf{T}_{ev}(s)\right\|_p=\left\|\mathbf{W}_O(s)\mathbf{T}_{zd}(s)\mathbf{W}_I(s)\right\|_p=\left\|\mathbf{W}_O(s)\mathcal{F}_\ell(\mathbf{P}(s),\mathbf{K}(s))\mathbf{W}_I(s)\right\|_p$$
$$\text{s.t. design constraints} \tag{10}$$

where $\|.\|_p$ refers to the H_2 or H_∞ system norm [14] (p=2 or ∞), while $\mathbf{W}_I$ and $\mathbf{W}_O$ are the input and output weights selected as proper stable transfer matrices of dimensions $\dim(\mathbf{d})\times\dim(\mathbf{v})$ and $\dim(\mathbf{e})\times\dim(\mathbf{z})$, respectively (for the problem formulated in Section 2.1: $\dim(\mathbf{d})=N+1$, $\dim(\mathbf{z})=2N$). Formal definitions, existence conditions and computational procedures for these H_2 and H_∞ weighted MIMO norms have been discussed in the Appendix.

As previously pointed out, the input weighting transfer matrix $\mathbf{W}_I$ enables us to take into account the relative magnitude and frequency content of the disturbance signals **d** consisting of base excitation (earthquake acceleration) and force loading (wind-induced forces to the floors), with a general form (assuming $\dim(\mathbf{v})=N+1$) of:

$$[\mathbf{W}_I(s)]_{(N+1)\times(N+1)}=\begin{bmatrix}W_{\mathrm{eq}}(s)_{1\times 1} & \mathbf{0}_{1\times N}\\ \mathbf{0}_{N\times 1} & \mathbf{W}_{\mathrm{ext}}(s)_{N\times N}\end{bmatrix} \tag{11}$$

where W_{eq} is the earthquake weighting filter and $\mathbf{W}_{\mathrm{ext}}$ is the weighting for the external forces to the floors. If the main purpose of the TMD system is vibration attenuation against earthquake, as is the case in the examples considered in this paper, $\mathbf{W}_{\mathrm{ext}}$ can be set to zero; then, the all-zero columns can be eliminated to yield the following simplified input weight:

$$[\mathbf{W}_I]_{(N+1)\times 1}=[W_{\mathrm{eq}}\quad \mathbf{0}_{1\times N}]^{\mathrm{T}} \tag{12}$$

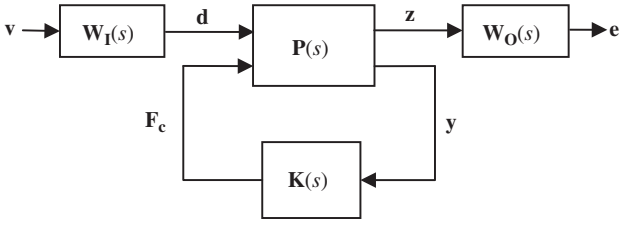

Fig. 5. Input–output weighted LFT configuration.

with dim($\mathbf{v}$)=1 (only base acceleration) and the earthquake weighting simply chosen as either 1 (no frequency content information) or

$$W_{eq}(s) = w_0 \frac{2\zeta_g \omega_g s + \omega_g^2}{s^2 + 2\zeta_g \omega_g s + \omega_g^2} \tag{13}$$

where ω_g and ζ_g are characteristic ground frequency and damping ratio, and w_0 is a scaling factor. This is a Kanai–Tajimi [32–34] shaping filter that leads the designed TMD system better be trained (during the optimization process) against an earthquake loading with a similar spectral content. The effect of this spectral content training will be illustrated in Section 5.1.2 with details and results. More complicated filters, such as the three stage filter used in [35], that enable a more detailed modeling of the ground dominant frequency and soil characteristics can also be similarly incorporated. Moreover, details on across-wind-excitation spectral loading can be found in the literature, e.g. [36,37], and can be used to form appropriate input weights for design against wind loadings.

The role of the output weight, on the other hand, is to specify the amount of the designer's emphasis on reducing each of the different error outputs $\mathbf{z}$ consisting of the inter-story drifts and absolute accelerations of the floors. The general form of this weighting, assuming dim($\mathbf{e}$)=$2N$, is

$$[\mathbf{W}_O(s)]_{2N\times 2N} = \begin{bmatrix} \mathbf{W}_{\mathrm{drf}}(s) & \mathbf{0}_{N\times N} \\ \mathbf{0}_{N\times N} & \mathbf{W}_{\mathrm{acc}}(s) \end{bmatrix} \tag{14}$$

with $\mathbf{W}_{\mathrm{drf}}$ and $\mathbf{W}_{\mathrm{acc}}$ as the drift and acceleration output filters. But, if the main focus is reduction of inter-story drifts (protection against structural damage), as is the case in all the design examples of Section 5, the following simplified output matrix weight (after elimination of all-zero rows) is a suitable choice:

$$[\mathbf{W}_{O1}]_{N\times 2N} = \begin{bmatrix} \mathbf{I}_{N\times N} & \mathbf{0}_{N\times N} \end{bmatrix} \tag{15}$$

with dim($\mathbf{e}$)=N (only inter-story drifts as target controlled quantities); otherwise, if the primary emphasis is reduction of floors absolute acceleration (protection against losses to the building contents), a simple choice would be as follows:

$$[\mathbf{W}_{O2}]_{N\times 2N} = \begin{bmatrix} \mathbf{0}_{N\times N} & \mathbf{I}_{N\times N} \end{bmatrix} \tag{16}$$

again with dim($\mathbf{e}$)=N but with the accelerations selected as target outputs.

The optimization problem, i.e. Eq. (10), might be solved by different methods. To overcome difficulties and disadvantages involved in methods such as exhaustive search (unreasonably low efficiency and high computational cost) and gradient-based methods (need for analytical formulation of the gradients, involved algorithmic complexities and convergence concerns that seriously restrict the span of treatable problems), genetic algorithm (GA) has been selected. Inspired from the concept of natural selection, GA shows a great promise of convergence to a nearly global optimum. GA can also easily handle design constraints in Eq. (10): bounds on design variables $\mathbf{x}$ are naturally incorporated, while other potential constrains on the TMD systems can be treated by penalty functions. Besides searching a descritized hypercube of real design variables, GA has also the ability to search a combinatorial space. This is due to the flexibility in the genetic coding and the independence to explicit parameterization of the objectives by design variables. This means that except for the TMDs specifications, the number, location and configuration of the TMD units can also be simultaneously optimized. Of course, exploiting all these possibilities is not the main purpose of this study. Due to these and other many advantages, genetic algorithms are well-established in the literature (see Ref. [38] for details on GA operators and implementation concepts), and widely used in various engineering problems including optimization of TMD systems [9,16,18,29].

4. The robust performance optimization problem

In the single objective optimization of the previous section, a perfect match between the model and actual structure was assumed that if violated might result in a significant degradation of the actual effectiveness of the designed TMD system. However, as explained in Section 1, this perfect match cannot be expected in practical situations due to the existing uncertainties. Uncertainty is generally categorized as aleatory (due to inherent variation) and epistemic (due to lack of exact knowledge). The former is usually modeled by random variables following specific probability distributions, while the latter is modeled by parameters each lying in a specific interval [39]. This section is intended to tackle robust optimization in the presence of generic multiple epistemic (interval) uncertainties. Section 4.1 deals with the simplest form of the uncertain problem assuming only a single real uncertain parameter. This provides a link to the previous robustness concepts in the literature and serves as a preamble to the much more complicated case of multiple-parameter uncertainty studied in Section 4.2.

4.1. Single-parameter uncertainty

The mismatch between natural frequencies of the actual structure and its model has a most significant detuning effect on the TMD system effectiveness. Hence, in this subsection, the single-parameter uncertainty is chosen as the following

uncertain perturbation to the structural stiffness matrix:

$$\mathbf{K}_{s\delta} = \mathbf{K}_{s,\mathrm{nom}}(1 + w_K\delta), \quad -1 \le \delta \le 1 \tag{17}$$

where $\mathbf{K}_{s,\mathrm{nom}}$ is the nominal stiffness matrix, $\mathbf{K}_{s\delta}$ is the perturbed structural stiffness matrix, w_K is the uncertainty level, and δ is the real parametric uncertainty. We shall also modify our notation $\mathbf{P}$ for the structural TITO system to $\mathbf{P}_{\mathrm{nom}}$ for the system resulting from $\mathbf{K}_{s,\mathrm{nom}}$ and $\mathbf{P}_\delta$ for that resulting from $\mathbf{K}_{s\delta}$; and consequently, a generalized weighted performance index for the uncertain structure can be defined as

$$J_P(\delta) = \left\| \mathbf{W}_O F_\ell(\mathbf{P}_\delta, \mathbf{K}) \mathbf{W}_I \right\|_p \tag{18}$$

based on which the previously defined nominal performance index J_{NP} would be

$$J_{\mathrm{NP}} = \left\| \mathbf{W}_O F_\ell(\mathbf{P}_{\mathrm{nom}}, \mathbf{K}) \mathbf{W}_I \right\|_p = J_P(0) \tag{19}$$

In Ref. [16], the authors showed that the behavior and flatness of the effectiveness curve versus the estimation error is a good qualitative concept of robustness against that error; and if quantified, yields a good measure of robustness. The same reasoning, if applied to $J_P(\delta)$, can lead to the following index J_R as a suitable index of robustness:

$$J_R = \left(\frac{1}{n_\delta + 1} \sum_{j=0}^{n_\delta} [J_P(\delta_j) - J_P(0)]^2 \right)^{1/2} \tag{20}$$

where $\delta_j = -1 + 2(j-1)/(n_\delta - 1)$ for $j = 1 \ldots n_\delta$ is a descritization of the uncertain parameter δ over its allowable range.

Due to the conflicting behaviors of robustness and nominal performance, as has been shown in [16], a good strategy is to formulate a two-objective optimization problem. Based on the indices proposed in this paper, this would be

$$\min_{\mathbf{x}} \begin{Bmatrix} J_{\mathrm{NP}} \\ J_R \end{Bmatrix} \quad \text{s.t.} \quad \text{design constraints} \tag{21}$$

where the solution for $\mathbf{x}$ (vector of design variables) will not be a single point $\mathbf{x}^*$ only; but a set of Pareto optimal points. A point $\mathbf{x}^*$ in the feasible design space $\mathbf{S}$ is called Pareto optimal if there is no other point $\mathbf{x}$ in the set $\mathbf{S}$ that dominates $\mathbf{x}^*$ (improves at least one objective function without degrading another one) [16]. An extremely appealing characteristic of GA is the potential to make the population converge to the Pareto optimal set incorporating a great number of possible non-dominated compromises between the two objectives. This is a further motivation, in addition to the reasons discussed in Section 3, to adopt GA in the current investigation. Details on multi-objective GA concepts and implementation can be found in literature [40], as well as different examples of implementation, also including TMD system design [9,16,29].

Another important issue is the concept of worst-case performance [5,9] which motivates the formulation of the following index based on $J_P(\delta)$ to characterize robust performance:

$$J_{\mathrm{WCP}} = \max_{\delta \ \text{allowable}} J_P(\delta) \simeq \max_{1 \le j \le n_\delta} J_P(\delta_j) \tag{22}$$

The worst-case performance index in Eq. (22) guarantees avoidance of overestimation and thus achievement of high robust performance, if utilized as the single objective or as the preference criterion to select a solution from all those obtained through the two-objective optimization (21). As will be discussed in Section 5.1.1, the two mentioned ways of utilizing J_{WCP} are very similar in terms of the final result. Therefore, if robust design is the main purpose, single objective worst-case performance minimization is preferred over two-objective minimization (21) due to the much lower computational cost (single objective GA runs need much smaller population sizes and less number of generations). The other appealing characteristic of the worst-case performance, specifically in the case of $p = \infty$, is that it can be generalized to the multiple-parameter case in a computationally efficient way. This is what we shall pursue in the next subsection.

4.2. Multiple-parameter uncertainty

Although the robustness concepts of the previous subsection can be directly generalized to the multiple-parameter uncertainty case, the exhaustive search over a fine descritized grid of the uncertain parameters hypercube is not a computationally acceptable method for more than two uncertain parameters. In this section, we shall focus on a computationally efficient way to assess the H_∞ worst-case performance index for the case of generic multiple-parameter uncertainty. Here, the theoretical background is much more involved [14,30] and a more complicated uncertainty modeling is required. Similarly as we did in Section 2 to isolate the TMD system dynamics from the plant, now we need to pull out the uncertainties in the plant parameters and collect them into the structured perturbation block $\mathbf{\Delta}$ within the LFT framework of Fig. 6.

According to this LFT interconnection, the mapping from excitation $\mathbf{v}$ to output $\mathbf{e}$ (we assume that any input or output weighting is absorbed into $\mathbf{P}$) is described as

$$\mathbf{T}_{ev}^{\Delta}(s) = \mathcal{F}_u(\mathcal{F}_\ell(\mathbf{P}, \mathbf{K}), \mathbf{\Delta}) = \mathcal{F}_u(\mathbf{M}, \mathbf{\Delta}) = \mathbf{M}_{ev} + \mathbf{M}_{er}\mathbf{\Delta}(I - \mathbf{M}_{hr}\mathbf{\Delta})^{-1}\mathbf{M}_{hv} \tag{23}$$

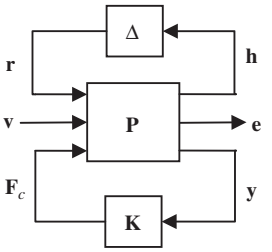

Fig. 6. LFT framework with the TMD system as the controller and the structured uncertainty.

Table 1
Multiple-parameter uncertainty illustrative scenario.

Uncertainty in the mass of all the floors	$m_i=\overline{m}_i(1+w_i\delta_i);\quad i=1,2,\ldots,N$ or in matrix form: $\mathbf{M}_s=\overline{\mathbf{M}}_s(\mathbf{I}+\mathbf{W}_M\mathbf{\Delta}_M)$ where $\mathbf{W}_M=\mathrm{diag}(w_1,\ldots,w_N),\quad \mathbf{\Delta}_M=\mathrm{diag}(\delta_1,\ldots,\delta_N)$
Uncertainty in the stiffness of the first floor	$k_1=\overline{k}_1(1+w_{N+1}\delta_{N+1})$
Uncertainty in the structural damping ratio	$\zeta=\overline{\zeta}(1+w_{N+2}\delta_{N+2})$

$-1\le\delta_i\le 1$ for i=1,2, …, N+2; w_i's represent the uncertainty level; and the bar symbol represents the nominal value.

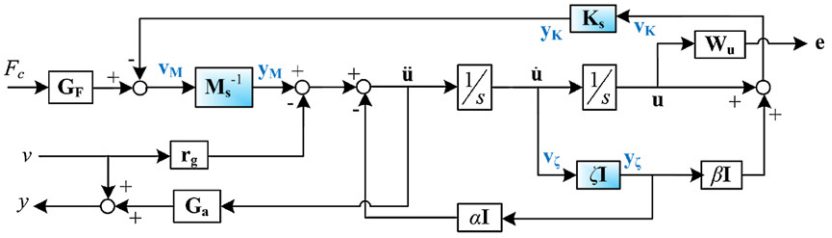

Fig. 7. Block diagram of the uncertain plant with uncertainties embedded in M_s^{-1}, K_s and ζI.

where a consistent partitioning of $\mathbf{M}=\mathcal{F}_\ell(\mathbf{P},\mathbf{K})$ is assumed. $\mathcal{F}_u(\mathbf{M},\mathbf{\Delta})$ has a useful interpretation: $\mathbf{M}_{ev}$ is the nominal mapping from $\mathbf{v}$ to $\mathbf{e}$ accomplished by the nominal structure–TMD system, and this nominal mapping is perturbed by $\mathbf{\Delta}$; $\mathbf{M}_{hr}$, $\mathbf{M}_{hv}$, and $\mathbf{M}_{er}$ reflect a priori knowledge on how the uncertainty affects the nominal map. Since the mapping from disturbance to target outputs includes all information required for characterizing the structure–TMD system performance, this LFT formulation seems quite promising. In particular, we are interested in calculating the following worst-case performance index:

$$J_{\mathrm{WCP},\infty}=\max_{\mathbf{\Delta}\ \text{allowable}}\left\|\mathbf{T}^{\Delta}_{ev}(j\omega)\right\|_\infty=\max_{\mathbf{\Delta}\ \text{allowable}}\left\|\mathcal{F}_u(\mathbf{M}(j\omega),\mathbf{\Delta})\right\|_\infty \tag{24}$$

At this point, two questions arise:

1) How to cast a given problem into this LFT framework?
2) How to calculate $J_{\mathrm{WCP},\infty}$ after having derived $\mathbf{M}$ and the structure of $\mathbf{\Delta}$ for our system?

The answer to the first question is a procedure referred to as pulling out the δ's that we shall illustrate through a generic example, while the second is related to mathematical theorems and numerical algorithms in the field of robust control that we will briefly discuss and cite at the end of this subsection.

Let us consider the N-story shear building with an n-MTMD on the top floor subjected to only base acceleration of unknown frequency content, i.e. $\mathbf{W}_I=[1\ \mathbf{0}_{1\times N}]^{\mathrm{T}}$, with only the inter-story drifts as target output quantities, see Eq. (15). Now assume the quite generic example of multiple parametric uncertainty described in Table 1.

It is easier to illustrate the procedure via block-diagram graphical representation. So consider the following rearrangement of Eq. (4) with a little change in notation, and its block-diagram representation in Fig. 7:

$$\begin{aligned}\ddot{\mathbf{u}}&=-\alpha\zeta\dot{\mathbf{u}}-\mathbf{M}_s^{-1}\mathbf{K}_s(\beta\zeta\dot{\mathbf{u}}+\mathbf{u})+\mathbf{M}_s^{-1}\mathbf{G}_F F_c-\mathbf{r}_g v\\ \mathbf{e}&=\mathbf{W}_u\mathbf{u},\quad y=\mathbf{G}_a\ddot{\mathbf{u}}+v\end{aligned} \tag{25}$$

where F_c=F_{MTMD}, v=a_g, β=2/(ω_1+ω_2), and α=$\beta\omega_1\omega_2$. Note that $\mathbf{G}_a$ and $\mathbf{G}_F$ have been absorbed from Eq. (8) for the MTMD into the plant, so that F_c and y are scalars and the MTMD block to be used as the controller $\mathbf{K}$ is SISO ($\mathbf{G}_a$ and $\mathbf{G}_F$ should be omitted from matrices $\mathbf{B}_K$ and $\mathbf{C}_K$ of the MTMD block in Eq. (8)).

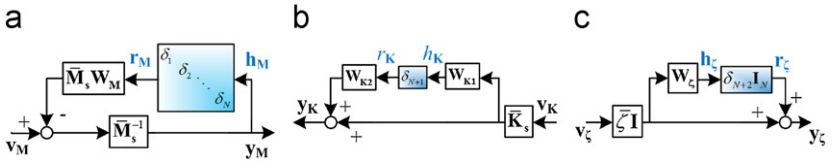

Fig. 8. Pulling out δ's from $\mathbf{M}_s^{-1}$, $\mathbf{K}_s$, and $\zeta\mathbf{I}$ blocks.

Now consider the blocks that embed the uncertainties (highlighted in Fig. 7). It is an easy task to check that these blocks can be expanded as shown in Fig. 8 to separate the nominal values and the uncertain perturbations. For example, Fig. 8b is the graphical equivalent of the following relation:

$$\begin{bmatrix} \bar{k}_1(1+w_{N+1}\delta_{N+1})+k_2 & -k_2 & & 0 \\ -k_2 & k_2+k_3 & \ddots & \\ & \ddots & & \\ 0 & & & k_N \end{bmatrix} = (\mathbf{I}+\mathbf{W}_{K2}\delta_{N+1}\mathbf{W}_{K1}) \begin{bmatrix} \bar{k}_1+k_2 & -k_2 & & 0 \\ -k_2 & k_2+k_3 & \ddots & \\ & \ddots & & \\ 0 & & & k_N \end{bmatrix} \tag{26}$$

where $\mathbf{W}_{K1}=[1\ 1\ \dots\ 1]$ and $\mathbf{W}_{K2}=[w_{N+1}\ 0\ \dots\ 0]^{\mathrm{T}}$. Also note that in Fig. 8c, $\mathbf{W}_\zeta=w_{N+2}\mathbf{I}_N$.

By combining Figs. 7 and 8, and graphically rearranging the signals and blocks, the following block diagram is obtained.

As can be seen, this block-diagram matches the LFT framework of Fig. 6. Accordingly, the structure of the uncertainty perturbation is $\mathbf{\Delta}=\mathrm{blkdiag}(\mathrm{diag}(\delta_1,\dots,\delta_{N+1}),\delta_{N+2}\mathbf{I}_N)$. Also, the model of the uncertainty pulled out plant with state vector $\mathbf{x}=[\mathbf{u}^{\mathrm{T}},\dot{\mathbf{u}}^{\mathrm{T}}]^{\mathrm{T}}$, three groups of inputs $\mathbf{r}=[\mathbf{r}_M^{\mathrm{T}},\mathbf{r}_K^{\mathrm{T}},\mathbf{r}_\zeta^{\mathrm{T}}]^{\mathrm{T}}$, v, and F_c, and the three groups of outputs $\mathbf{h}=[\mathbf{h}_M^{\mathrm{T}},\mathbf{h}_K^{\mathrm{T}},\mathbf{h}_\zeta^{\mathrm{T}}]^{\mathrm{T}}$, $\mathbf{e}$, and y is as follows:

$$\mathbf{P}=\left[\begin{array}{c|ccc} \mathbf{A} & \mathbf{B}_r & \mathbf{B}_v & \mathbf{B}_F \\ \hline \mathbf{C}_h & \mathbf{D}_{hr} & \mathbf{D}_{hv} & \mathbf{D}_{hF} \\ \mathbf{C}_e & \mathbf{D}_{er} & \mathbf{D}_{ev} & \mathbf{D}_{eF} \\ \mathbf{C}_y & \mathbf{D}_{yr} & \mathbf{D}_{yv} & \mathbf{D}_{yF} \end{array}\right] \tag{27}$$

It is easy to verify that all the matrices without a subscript r or h are defined based on the nominal values as if there was no uncertainty, while those with these subscripts can be derived as follows:

$$\mathbf{B}_r=\begin{bmatrix} \mathbf{0} & \mathbf{0} & \mathbf{0} \\ -\mathbf{W}_M & -\bar{\mathbf{M}}_s^{-1}\mathbf{W}_{K2} & -\alpha\mathbf{I}-\beta\bar{\mathbf{M}}_s^{-1}\bar{\mathbf{K}}_s \end{bmatrix}$$

$$\mathbf{C}_h=\begin{bmatrix} -\bar{\mathbf{M}}_s^{-1}\bar{\mathbf{K}}_s & -\bar{\zeta}\beta\bar{\mathbf{M}}_s^{-1}\bar{\mathbf{K}}_s \\ \mathbf{W}_{K1}\bar{\mathbf{K}}_s & \bar{\zeta}\beta\mathbf{W}_{K1}\bar{\mathbf{K}}_s \\ \mathbf{0} & \bar{\zeta}\mathbf{W}_\zeta \end{bmatrix},\quad \mathbf{D}_{hr}=\begin{bmatrix} -\mathbf{W}_M & -\bar{\mathbf{M}}_s^{-1}\mathbf{W}_{K2} & -\beta\bar{\mathbf{M}}_s^{-1}\bar{\mathbf{K}}_s \\ \mathbf{0} & 0 & \beta\mathbf{W}_{K1}\bar{\mathbf{K}}_s \\ \mathbf{0} & \mathbf{0} & \mathbf{0} \end{bmatrix}$$

$$\mathbf{D}_{hv}=\mathbf{0},\quad \mathbf{D}_{hF}=\begin{bmatrix} \bar{\mathbf{M}}_s^{-1}\mathbf{G}_F \\ \mathbf{0} \end{bmatrix},\quad \mathbf{D}_{er}=\mathbf{0}$$

$$\mathbf{D}_{yr}=\begin{bmatrix} -\mathbf{G}_a\mathbf{W}_M & -\mathbf{G}_a\bar{\mathbf{M}}_s^{-1}\mathbf{W}_{K2} & -\mathbf{G}_a(\alpha\mathbf{I}+\beta\bar{\mathbf{M}}_s^{-1}\bar{\mathbf{K}}_s) \end{bmatrix}$$

Now we shall address the second question posed at the beginning of this subsection. Let us take a closer look at Eq. (24) for $J_{\mathrm{WCP},\infty}$ and do some manipulations:

$$\begin{aligned} J_{\mathrm{WCP},\infty} &= \max_{\mathbf{\Delta}\ \text{allowable}} \left\| \mathcal{F}_u(\mathbf{M}(j\omega),\mathbf{\Delta}) \right\|_\infty = \max_{\mathbf{\Delta}\ \text{allow}} \max_{\omega} \bar{\sigma}[\mathcal{F}_u(\mathbf{M}(j\omega),\mathbf{\Delta})] \\ &= \max_{\omega} \max_{\mathbf{\Delta}\ \text{allow}} \bar{\sigma}[\mathcal{F}_u(\mathbf{M}(j\omega),\mathbf{\Delta})] \simeq \max_{1\le i\le N_\omega} \left(\max_{\mathbf{\Delta}\ \text{allow}} \bar{\sigma}[\mathcal{F}_u(\mathbf{M}(j\omega_i),\mathbf{\Delta})] \right) \end{aligned} \tag{28}$$

where $\bar{\sigma}$ denotes the greatest singular value. First the maximizations have been interchanged, then the frequency range is discretized to N_ω grids. At each frequency ω_i, $\mathbf{M}(j\omega_i)$ is a constant complex matrix. This implies that we can focus on the constant matrix problem (the maximization inside the parentheses in the last expression), and re-solve at each frequency. In the robust control literature, there are investigations zooming on approximate solutions for the constant matrix problem. A well-known algorithm [30] uses the divide and conquer strategy based on upper and lower bounds for this problem. The lower bound is computed through an iterative procedure that mimics Hamiltonian methods for state-space norm calculations in its substeps. The upper bound calculation, on the other hand, is based on a LMI formulation. To obtain $J_{\mathrm{WCP},\infty}$, such a procedure should be repeated over the frequency grid. However, since the peak-over-frequency is of interest, large frequency ranges can be quickly eliminated in order to reduce the computation time. Ref. [41] discusses relevant software implementation.

The formulation developed in this section unifies the robust design of passive TMD systems for structures with multiple uncertainties with the rigorous SSV (μ) framework in robust control (see Ref. [42] for a relevant example of active structural control). Besides real parametric uncertainty, this framework can also handle other types of uncertainties such

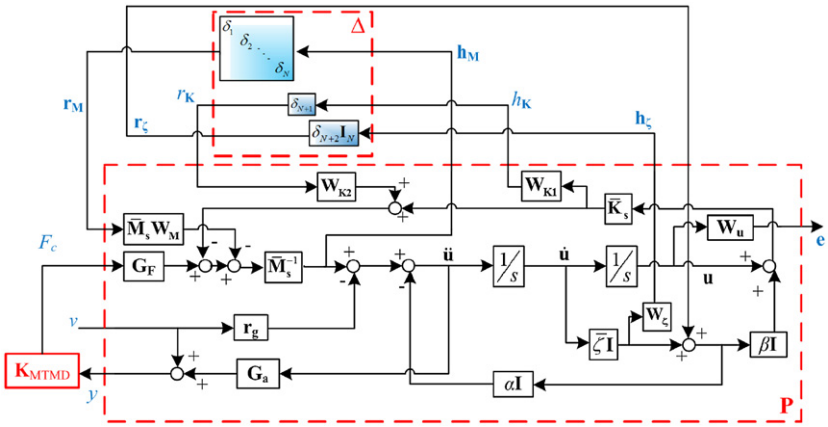

Fig. 9. Block diagram of the uncertain plant–TMD system with uncertainties pulled out.

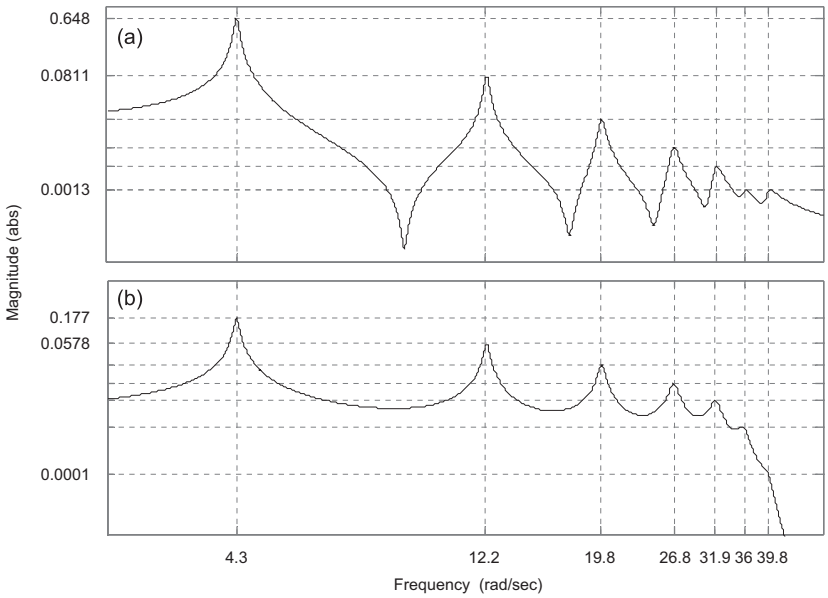

Fig. 10. FRF of the uncontrolled building from ground acc. to inter-story drifts of the first (a) and top floors (b).

as the neglected dynamics introducing complex uncertainty blocks into Δ. Of course, this type of uncertainty is more relevant to active control where high-frequency neglected dynamics can have detrimental effects on system characteristics such as stability and noise immunity. The advantage of this unification is the possibility to adopt previously developed methods and inspire from ideas in the robust control literature for design of passive vibration absorbers as has been demonstrated in this section (Fig. 9).

5. Implementation examples

This section demonstrates how easily the method can be implemented on various problems with different assumptions, and illustrates the post-processing step of the proposed framework (Fig. 1).

The structural model considered for all examples of this section is a 7-storied shear building with the following nominal structural properties: $\mathbf{k}=[2.5,2.5,2.5,2\ 2\ 2\ 2]\times 10^7$ (N/m), $\mathbf{m}=5.5\times 10^4\times[1,1,\ldots,1]$ (kg) and $\zeta_s=0.01$. The building is excited only by ground acceleration, and its frequency response (in terms of the inter-story drifts of the first and top floors) is depicted in Fig. 10. The structural mode peaks and frequencies have been also clearly illustrated.

In the GA optimization, the non-dimensionalized parameters of the TMD units have been used as design variables. Assuming equal distribution of the total TMD system mass, the design variables vector x will comprise the frequency ratios β_i and damping ratios ζ_i of the TMD units which can be conveniently searched within reasonably predictable bounds.

The parameters of the TMD units in the formulation of Section 2.2 can then be computed as

$$m_{T,i} = \mu_i \times m_{s,tot}, \quad k_{T,i} = m_{T,i}(\beta_i \omega_{s1})^2, \quad c_{T,i} = 2\zeta_i \sqrt{m_{T,i} k_{T,i}}, \quad \mu_i = \mu_{tot}/n \tag{29}$$

where n is the total number of TMD units; μ_{tot} is the ratio of the total mass of the TMD system to the total mass of the building $m_{s,\text{tot}}$; and ω_{s1} is the first natural frequency of the building.

5.1. Single-parameter uncertainty examples

Several design examples will be considered in this subsection, each having a different combination of TMD system specifications and minimization objectives. Of course, all the examples assume the single-parameter uncertainty (17) with w_k=0.05. All these cases (designs I, II, …, V) are listed and summarized in Table 3 along with their respective assumptions. Each design example requires a two-objective GA run as described by Eq. (22). For instance, design I that is the typical central example (with which all other designs are compared) has been obtained by a GA run described in Table 2.

The minimization objectives J_{NP} and J_R are defined based on $J_P(\delta)$ defined in Eq. (18) applying Eqs. (19) and (20), respectively. According to the designer's purpose, different types of norm, and input/output weights can be assumed for $J_P(\delta)$. In this study 3 different definitions for $J_P(\delta)$ are considered as listed in Table 3.

5.1.1. Different TMD system specifications

To study the influence of the TMD system specifications on its effectiveness–robustness characteristics, in this subsection, an IMTMD on top floor (Design I), a UMTMD on top floor (Design II), and the "STMD on every floor" configuration (Design III) are designed as described in Table 3. The resulting Pareto fronts in the criterion space are compared in Fig. 11.

The Pareto front of an STMD on top floor has been also included in Fig. 11 for further comparison. As can be seen, the UMTMD system (with 3 design variables) dominates the STMD system (with 2 design variables), mostly in terms of nominal performance. Similarly, the IMTMD (with 14 design variables) dominates the UMTMD; this advantage is most significant in the high robustness (low J_R) region. In other words, irregular design enables us to design a highly robust MTMD system with considerably lower sacrifice of nominal performance. Finally, Design III dominates all previous designs by exploiting the "STMD on every floor" configuration that physically allows the installation of an overall heavier TMD

Table 2
Specifications of GA run for design I.

Algorithm type	Two branch tournament
Minimization objectives	J_{NP} and J_R defined based on $J_{P1}(\delta)$
Population size	500
Pareto fraction	0.4
Number of generations	400
Cross-over	
Type	Scattered
Prob.	0.8
Mutation probability	0.05

Table 3
Specifications of design examples of Section 5.1.

#	TMD system specifications	Minimization objectives J_{NP} and J_R defined based on	Section
I	Irregular MTMD, n=7, μ_{tot}=0.03 $\mathbf{x}=\begin{bmatrix}\beta_1 & \cdots & \beta_7 & \zeta_1 & \cdots & \zeta_7\end{bmatrix}^{\text{T}}$	$J_{P1}(\delta)=\|\mathbf{W}_{O1}\mathcal{F}_\ell(\mathbf{P}_\delta,\mathbf{K})\begin{bmatrix}1\\ \mathbf{0}_{N\times 1}\end{bmatrix}\|_\infty$ [b]	5.1.1/2
II	Uniform MTMD, n=7, μ_{tot}=0.03 $\mathbf{x}=\begin{bmatrix}\Delta\beta & \beta_o & \zeta\end{bmatrix}^{\text{T}}$ [a]	$J_{P1}(\delta)$	5.1.1
III	STMD on every floor, μ_{tot}=0.06 $\mathbf{x}=\begin{bmatrix}\beta_1 & \cdots & \beta_7 & \zeta_1 & \cdots & \zeta_7\end{bmatrix}^{\text{T}}$	$J_{P1}(\delta)$	5.1.1
IV	Irregular MTMD, n=7, μ_{tot}=0.03 $\mathbf{x}=\begin{bmatrix}\beta_1 & \cdots & \beta_7 & \zeta_1 & \cdots & \zeta_7\end{bmatrix}^{\text{T}}$	$J_{P2}(\delta)=\|\mathbf{W}_{O1}\mathcal{F}_\ell(\mathbf{P}_\delta,\mathbf{K})\begin{bmatrix}W_{\text{eq1}}\\ \mathbf{0}_{N\times 1}\end{bmatrix}\|_\infty$ [c]	5.1.2
V	Irregular MTMD, n=7, μ_{tot}=0.03 $\mathbf{x}=\begin{bmatrix}\beta_1 & \cdots & \beta_7 & \zeta_1 & \cdots & \zeta_7\end{bmatrix}^{\text{T}}$	$J_{P3}(\delta)=\|\mathbf{W}_{O1}\mathcal{F}_\ell(\mathbf{P}_\delta,\mathbf{K})\begin{bmatrix}W_{\text{eq2}}\\ \mathbf{0}_{N\times 1}\end{bmatrix}\|_\infty$ [d]	5.1.2

[a] UMTMD—$\Delta\beta$: total range of TMDs frequency ratio, β_o: offset of the central TMD frequency ratio $\beta_1=1+\beta_o-\Delta\beta/2$, $\beta_i=\beta_{i-1}+\Delta\beta/n (i=2\ldots7)$, $\zeta_i=\zeta (i=1\ldots7)$.
[b] W_{O1} as defined in Eq. (15).
[c] $W_{\text{eq1}}=W_{\text{eq}}|\{\omega_g=3\,\text{rad/s},\ \zeta_g=0.3\}$ (Eq. (13)).
[d] $W_{\text{eq2}}=W_{\text{eq}}|\{\omega_g=12\,\text{rad/s},\ \zeta_g=0.6\}$ (Eq. (13)).

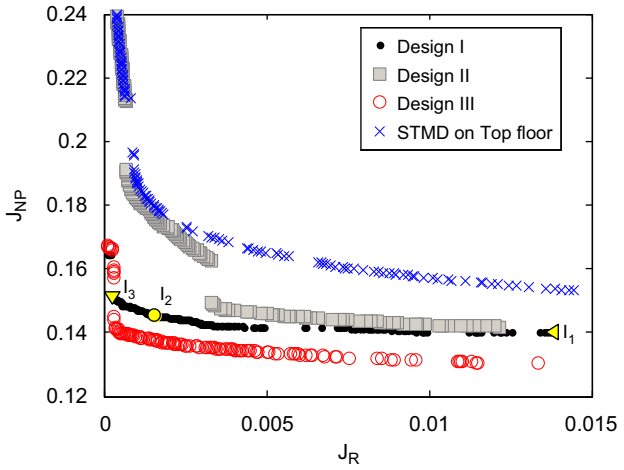

Fig. 11. Visualization of design sets in criterion space based on $J_{P1}(\delta)$.

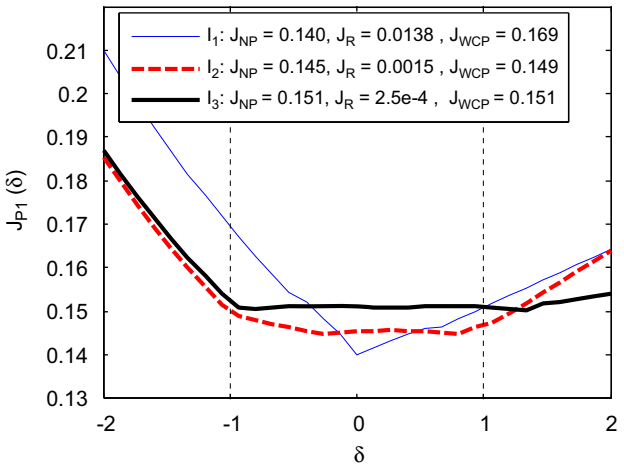

Fig. 12. Behavior of $J_{P1}(\delta)$ against δ for three design solutions.

system on the building (a numerical value of μ_{tot}=0.06 compared to μ_{tot}=0.03 is used in these examples). It is important to point out the significant effect of μ_{tot}: if the "STMD on every floor" system were designed with μ_{tot}=0.03, it would be dominated even by the STMD on top floor.

Now, let us analyze the trade-off between nominal performance and robustness by selecting three design points I_1, I_2, and I_3 on the Pareto curve I as shown in Fig. 11. These design points correspond to specific IMTMD system designs: I_1 is the most effective; I_3 is highly robust; and, I_2 achieves the best worst-case performance, i.e. the least value of J_{WCP} in Eq. (22) on the Pareto curve I. The $J_P(\delta)$-curves corresponding to these design points are illustrated in Fig. 12.

As can be seen from Fig. 12, design point I_1, being the most effective design under nominal conditions, is the most sensitive to uncertainty. On the other hand, the curve corresponding to design point I_3 is the flattest (the most robust in terms of J_R); but, it is less effective than I_2 in the entire uncertainty range of interest. In this sense, the design point I_2 is preferred to I_3 for achieving robust performance in the presence of uncertainty. Accordingly, minimizing the worst-case performance J_{WCP} is an appropriate preference criterion for choosing a robust solution from the entire set of $J_{NP}-J_R$ optimal set. This would yield a solution close to the solution obtained by direct single objective minimization of J_{WCP}. Indeed, the interesting advantage of two-objective optimization is that it results in an entire set of Pareto optimal solutions that incorporate a broad spectrum of design options. Of course, the designer should decide whether or not obtaining such a spectrum of designs justifies the augmented computational cost of two-objective optimization.

To further illustrate the characteristics of the two preferred TMD systems designs for achieving nominal (I_1) and robust (I_2) performance, the uncertain frequency responses (from ground acceleration to the inter-story drifts of the first and top floors) have been depicted in Fig. 13. This figure shows that the robust design manifests lower sensitivity to the variation of the uncertain parameter (of course, the difference is not dramatic because the level of uncertainty is low). In order to find

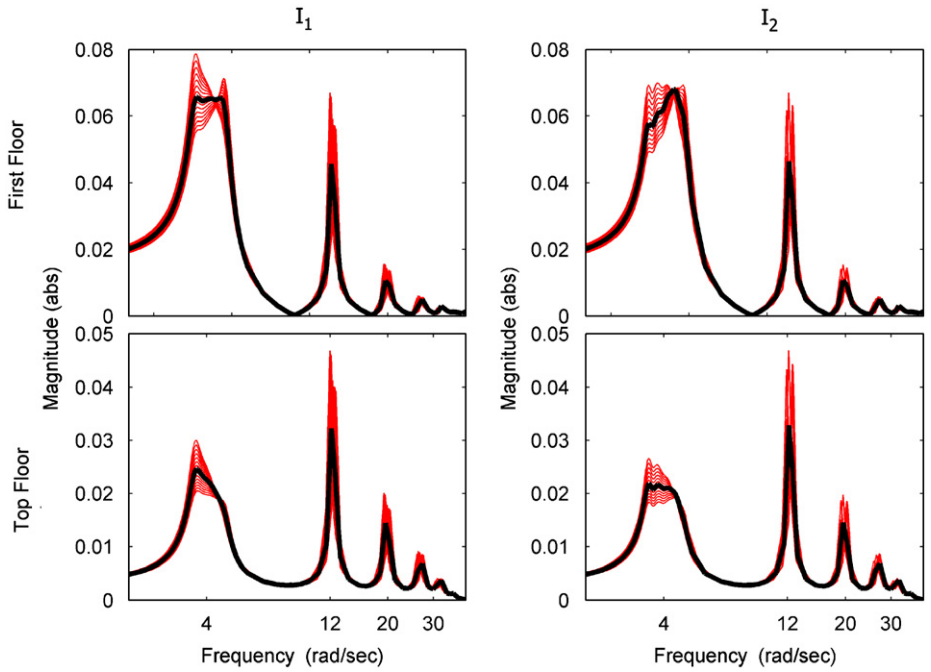

Fig. 13. Uncertain FRFs (from ground acc. to the inter-story drifts of the first and top floors) for two designs $\mathbf{I}_1$ and $\mathbf{I}_2$ (thick black curve: nominal response and red curves: uncertain samples).

out the amount of vibration suppression accomplished by TMD systems I_1 and I_2, it is useful to compare this figure to Fig. 10 that shows the uncontrolled building FRF.

5.1.2. Different frequency contents of excitation

A priori knowledge of the exact disturbance signal (or signals) is not available for design of the TMD system. Indeed, mitigation of the unknown disturbance is the primary task expected from the TMD system as a vibration controller. However, some information on the frequency content of the potential excitations might be available a priori; and we should try to take most possible advantage out of this information. For seismic vibration control, the ground excitation can be modeled by a stationary stochastic process with a spectral content of the form proposed by Kanai [43] and Tajimi [44], as previously presented in Eq. (13). In this subsection, the advantage of introducing such information into the design process will be investigated. Two spectra denoted by W_{eq1} (ω_g=3 rad/s, ζ_g=0.3) and W_{eq2} (ω_g=12 rad/s, ζ_g=0.6) in Table 3 (with ground frequencies near the first and second structural frequencies) are considered in this study, as shown in Fig. 14. These spectra [33] match the frequency contents of Uemachi (a simulated ground motion using fault rupture model) and El-Centro (the well-known seismic event recorded during the Imperial Valley, California earthquake of May 18, 1940); and, are utilized in the definition of $J_{P2}(\delta)$ (Designs IV) and $J_{P3}(\delta)$ (Design V), respectively.

The Design sets IV and V in $J_{\text{NP}}-J_R$ criterion spaces based on $J_{P2}(\delta)$ (with W_{eq1} as the input weight) and $J_{P3}(\delta)$ (with W_{eq2} as the input weight) have been respectively shown in Fig. 15a and b, along with Design set I for comparison. At the first glance, these visualizations might seem ambiguous and require clarification. For each design set, two criterion spaces can be considered: one utilized for optimization, and the other used for visualization. Consider Design set IV, for instance, where J_{NP} and J_R based on $J_{P2}(\delta)$ have been utilized as objectives for optimization. In Fig. 15a, this design set has been visualized in the same criterion space as has been optimized; hence, it constitutes a Pareto front of non-dominated solutions in this space. In Fig. 15b, on the other hand, Design IV has been visualized in a different criterion space (the criterion space based on $J_{P3}(\delta)$); consequently, it does not constitute a non-dominated Pareto front in this space. The opposite holds for Design set V; while, design I, in both subfigures, is visualized in criterion spaces different from the optimization space. Obviously, a post-processing (re-computation of objective indices) is required for visualization of a design curve in a criterion space different from its original optimization space. This post-processed visualization enables us to exactly assess the improvement of the effectiveness–robustness characteristics of the TMD system due to appropriate consideration of excitation spectral content and vice versa, i.e. the degradation effect due to not considering or inappropriately accounting for the frequency content of the disturbance.

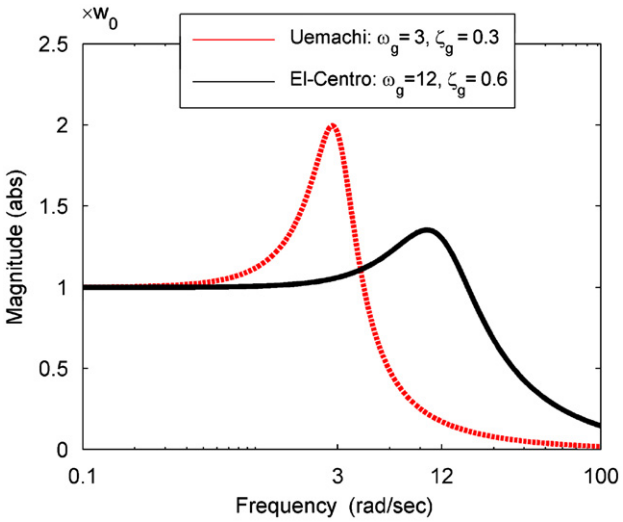

Fig. 14. Kanai–Tajimi filters used in Designs IV and V.

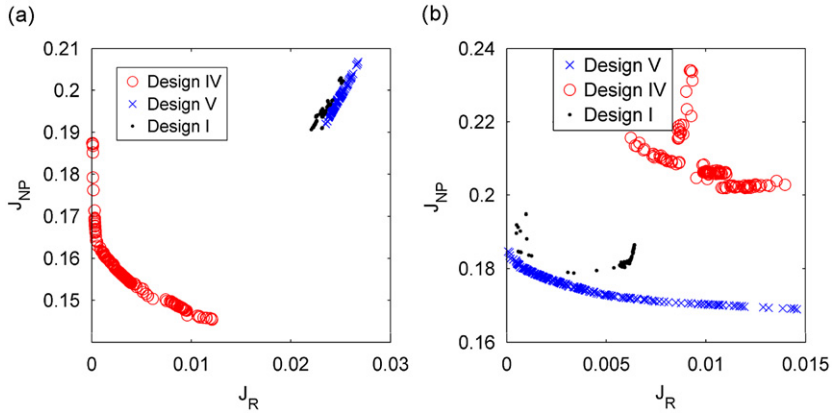

Fig. 15. Visualization of design sets in criterion space based on (a) $J_{P2}(\delta)$ and (b) $J_{P3}(\delta)$.

Compared to Design IV, Design V is closer to Design I in both criterion spaces (Fig. 15 a and b); in other words, influence of W_{eq1} on the design is more significant than W_{eq2} as its shape shows more deviation from the constant (frequency-independent) filter $W_{eq}=1$ used in Design I.

Now, for final assessment and validation, let us analyze the efficacy of the designs by time-response simulations. The most effective points IV_1 and V_1 (from Designs IV and V) are selected and compared to the most effective design point I_1 (from the previous subsection) in terms of the first floor inter-story drift response under nominal conditions. For performance evaluation of these designs against seismic excitations with frequency content similar to the Uemachi scenario, response to stationary stochastic process has been simulated. Such a random signal is generated by filtering a white noise through W_{eq1} and then scaling to achieve a peak ground acceleration (PGA) of 0.5 g. Fig. 16 shows a sample of such a simulation. Final performance evaluation can be carried out by comparison of the peak and rms reduction of random vibrations that each design accomplishes. Table 4 presents the final results averaged over 1000 simulations:

As expected according to the previous observations from Fig. 15, the results of Table 4, by random vibration analysis in time domain, show that consideration of consistent frequency content (Design IV) improves the result compared to when no frequency information is taken into account (Design I) or inconsistent information is used (Design V); where in the latter case, the result is even worsened. This statement proves again true (by interchanging IV↔V) for the case of W_{eq2} frequency content. This time validation is carried out via deterministic simulation against the El-Centro historical earthquake record, in Fig. 17. Although the improvements are moderate, the designs cannot be considered truly optimal if these improvements are not applied.

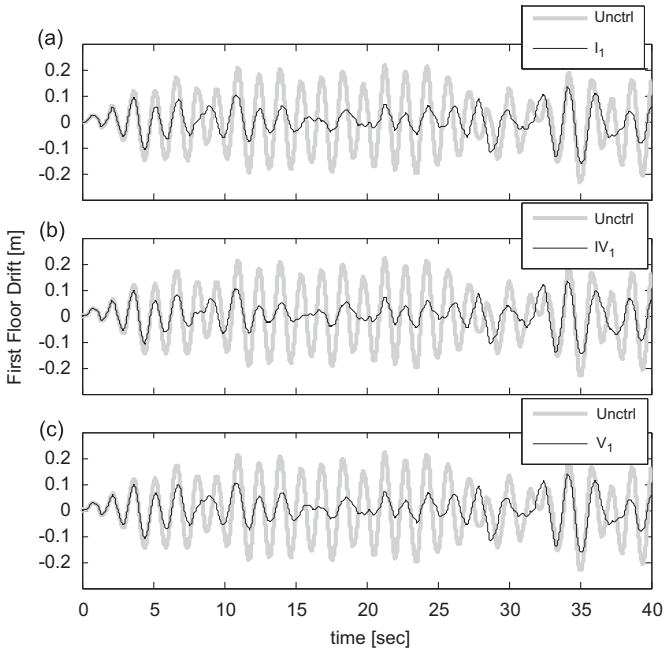

Fig. 16. A sample time-response to random noise colored by Uemachi filter. (a) Design point I_1—peak reduction: 32.3%; rms reduction: 53.7%. (b) Design point IV_1—peak reduction: 37.5%; rms reduction: 54.6%. (c) Design point V_1—peak reduction: 30.4%; rms reduction: 53%.

Table 4
Random vibration analysis results (Uemachi).

Reduction of:	**Design I_1** (%)	**Design IV_1** (%)	**Design V_1** (%)
Response peak	35.7	**37.1**	34.6
Response rms	40.4	**42.2**	39.3

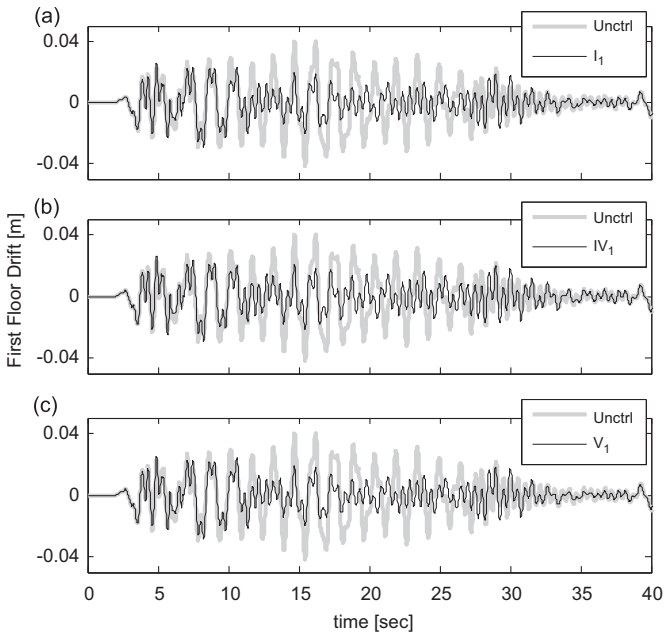

Fig. 17. Time-response to El-centro earthquake record. (a) Design point I_1—peak reduction: 29.9%; rms reduction: 39%. (b) Design point IV_1—peak reduction: 29.1%; rms reduction: 36.8%. (c) Design point V_1—peak reduction: 31.4%; rms reduction: 39.7%.

5.2. Multiple-parameter uncertainty example

Consider the 7-storied shear building subject to the multiple-parameter uncertainty described in Table 1 with $w_1=w_2=\cdots=w_7=0.1$, $w_8=0.2$, and $w_9=0.75$. Let us set up a single objective GA for designing an irregular 7-MTMD (14 design variables), once with $J_{NP,\infty}$ as the single objective (nominal design), and once with $J_{WCP,\infty}$ (robust design). All the assumptions and formulations follow the example of Section 4.2. The resulting MTMD designs (the damping and frequency ratios of the 7 TMD units) have been compared in Fig. 18. Due to the irregularity of the design and several number of influencing factors, specific results should not be generalized. However, there is a reasonable trend that can be generalized: more robust MTMD designs cover a broader frequency range and tend to have more damping.

The FRF of the building equipped with each individual MTMD design has been shown in Fig. 19. The FRF of the robust design manifests lower sensitivity to uncertainties, especially near the second mode of vibration which is the critical frequency.

Table 5 lists the numerical value of the nominal and worst-case performance indices for the two designs. As can be seen, the nominal design can suffer up to a 200% increase of gain (worst-case gain compared to the nominal gain) due to uncertainties; while, the gain increase for the robust design is at most 46%. Interestingly, for the building controlled by the robust MTMD, the critical frequency associated with the worst-case gain is near the second mode of vibration, while the nominal peak gain occurs at the first mode. For the building with the nominally optimal MTMD both peaks occur near the second mode.

The worst-case combination of parameters happens for $\delta_1=\delta_2=\delta_5=\delta_7=1$ and $\delta_3=\delta_4=\delta_5=\delta_8=\delta_9=-1$. It corresponds to the least allowable stiffness of the first story and structural damping, and a distribution of the mass of the floors that favors the second vibrational mode-shape (least allowable mass for the 3 floors in the middle, and the maximum allowable for the others). An interesting fact about this worst-case scenario is that it has happened at a corner of the uncertain parameters cube. Based on experience with several numerical simulations, the authors suspect that this is true for any problem of the generic class considered in this paper. This can avoid the cost and complexity involved with computing the worst-case gain bounds, and would lead to the exact value. The worst-case combination of parameters that the existing algorithms, e.g. the function *wcgain* in MATLAB Robust Control Toolbox [45], report is just the parameter combination attained at the end of the iterative search procedure for computing the lower bound on the worst-case gain. For the problem at hand, this will not always yield a corner; but, numerical experiments on this problem have shown that searching only the corners always improves (or at least, maintains) the result obtained from the lower bound procedure. However, no relevant theoretical grounding has been found in the literature. Hence, if theoretical guarantee is required, the divide and conquer strategy based on upper and lower bounds must be carried out.

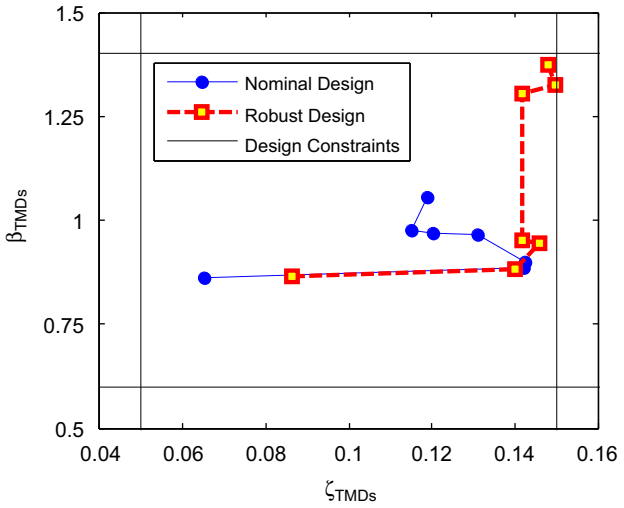

Fig. 18. Comparison of the nominal and robust designs in terms of design variables (damping and frequency ratios of the TMD units).

Table 5
Comparison of the nominal and robust designs in terms of performance indices.

	Nominal design	**Robust design**
Nominal performance ($J_{NP,\infty}$)	$0.1405@\omega_{cr}=12.28$ rad/s	$0.2278@\omega_{cr}=4.30$ rad/s
Worst-case performance ($J_{WCP,\infty}$)	$0.4215@\omega_{cr}=11.75$ rad/s	$0.3325@\omega_{cr}=11.76$ rad/s

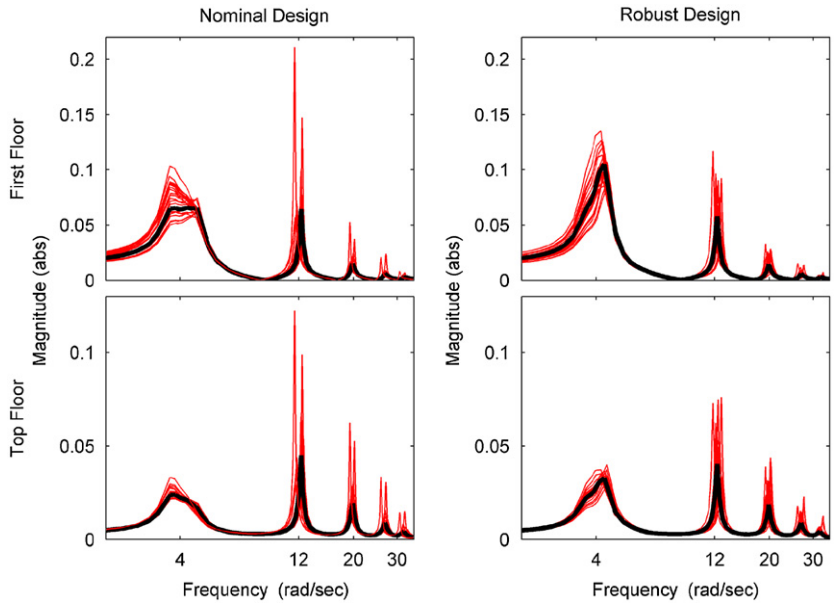

Fig. 19. Uncertain FRFs (from ground acc. to inter-story drifts of the first and top floors) for nominal and robust designs (thick black curve: nominal response and red curves: uncertain samples).

6. Conclusions

Toward establishing the proposed generalized framework for robust optimal design of TMD systems, the following primary contributions and results have been presented:

1) *The LFT formulation*: A rigorous LFT formulation has been introduced that isolates the TMD system as a feedback controller and the uncertainties as a structured block perturbing the nominal dynamics. It has been shown that this formulation can accommodate a general structure with any TMD system configuration and multiple-parameter uncertainty.
2) *Generalized performance indices for optimization*: The concept of weighted MIMO norms from external disturbance inputs to control-target quantities has been used as the most general measure of performance. In this way, knowledge about the frequency content of the excitations can be incorporated and the H_2 or H_∞ optimization of structural response in terms of different quantities (inter-story drifts or floor accelerations) can be formulated in a unified manner. A nominal performance index, a robustness index and a worst-case performance index have been formulated accordingly. The latter index in conjunction with the structured uncertainty modeling strategy has been shown to be efficiently computable in the presence of multiple-parameter uncertainty.
3) *Exploitation of evolutionary heuristics*: Advantages of exploiting evolutionary heuristics were demonstrated through implementation of GA optimization.
4) *Assumptions on the TMD system*: Comparison of IMTMD and UMTMD solution sets, designed to be installed on the top floor of a multi-story building, have demonstrated domination (in terms of effectiveness–robustness Pareto optimality) of irregular design, quite significant in the high robustness region. It has been also shown that by spatial distribution of the TMD units using a simple configuration of "STMD on every floor", a totally heavier and hence dominant TMD system can be exploited.
5) *Frequency content of excitation*: Consideration of frequency content information, through application of input weighting filters, has been shown to improve effectiveness–robustness characteristics of the TMD systems against excitations of consistent spectral content. Accordingly, a seismological study on the site plan of implementation and an estimation of the wind loadings spectral content can be beneficial to the TMD system design.
6) *The active control perspective toward passive optimization*: Application of ideas in active control theory for passive design of TMD systems has proved particularly beneficial: it has enabled the development of a flexible and rigorous formulation and utilization of worst-case performance assessment algorithms previously developed in robust control literature (far more superior than exhaustive search and existing Monte Carlo methods available for passive optimization). In a more general sense, the present paper can be considered a first step toward unification of passive and active TMD systems design in view of robust control. Future research in this context can involve simultaneous synthesis of the passive mechanical parameters and the control law for active TMD systems, or utilization of fixed-structure active control synthesis schemes for design of passive TMD systems (e.g. instead of the GA optimization scheme).

Appendix. Formal definitions and computation of the weighted MIMO norms

Consider the general input–output weighted LFT configuration of Fig. 5 formulated as the cascade interconnection of the input weight, the non-weighted LFT and the output weight:

$$\begin{aligned}\mathbf{T}_{ev}(s) &= \mathbf{W}_O(s)\,\mathcal{F}_\ell\big(\mathbf{P}(s),\mathbf{K}(s)\big)\,\mathbf{W}_I(s)\\ &= \left[\begin{array}{c|c}\mathbf{A}_O & \mathbf{B}_O\\ \hline \mathbf{C}_O & \mathbf{D}_O\end{array}\right]\left[\begin{array}{c|c}\mathbf{A}_{CL} & \mathbf{B}_{CL}\\ \hline \mathbf{C}_{CL} & \mathbf{D}_{CL}\end{array}\right]\left[\begin{array}{c|c}\mathbf{A}_I & \mathbf{B}_I\\ \hline \mathbf{C}_I & \mathbf{D}_I\end{array}\right]=\left[\begin{array}{c|c}\mathbf{A}_a & \mathbf{B}_a\\ \hline \mathbf{C}_a & \mathbf{D}_a\end{array}\right]\end{aligned} \tag{A-1}$$

according to the state-space realizations of the input and output weighting filters; the state-space matrices for the (non-weighted) LFT configuration described by Eq. (3-II); and, the resulting augmented matrices for the weighted LFT configuration, described as

$$\mathbf{A}_a=\begin{bmatrix}\begin{bmatrix}\mathbf{A}_O & \mathbf{B}_O\mathbf{C}_{CL}\\ \mathbf{0} & \mathbf{A}_{CL}\end{bmatrix} & \begin{bmatrix}\mathbf{B}_O\mathbf{D}_{\mathrm{CL}}\\ \mathbf{B}_{CL}\end{bmatrix}\mathbf{C}_I\\ \mathbf{0} & \mathbf{A}_I\end{bmatrix},\quad \mathbf{B}_a=\begin{bmatrix}\begin{bmatrix}\mathbf{B}_O\mathbf{D}_{CL}\\ \mathbf{B}_{CL}\end{bmatrix}\mathbf{D}_I\\ \mathbf{B}_I\end{bmatrix}$$

$$\mathbf{C}_a=\begin{bmatrix}\mathbf{C}_O & \mathbf{D}_O\mathbf{C}_{CL} & \mathbf{D}_O\mathbf{D}_{CL}\mathbf{C}_I\end{bmatrix},\quad \mathbf{D}_a=\mathbf{D}_O\mathbf{D}_{CL}\mathbf{D}_I$$

This augmented system $\mathbf{T}_{ev}(s)$, a stable structural plant controlled by a passive mechanical controller and weighted through proper stable filters, is a proper and real rational stable transfer matrix ($\in \mathcal{RH}_\infty$); hence, its H_∞ norm exists and is defined as [14]:

$$\|\mathbf{T}_{ev}\|_\infty=\sup_{\mathrm{Re}(s)>0}\overline{\sigma}[\mathbf{T}_{ev}(s)]=\sup_{\omega\in\mathbb{R}}\overline{\sigma}[\mathbf{T}_{ev}(j\omega)] \tag{A-2}$$

with $\overline{\sigma}$ denoting the greatest singular value. Furthermore, $\mathbf{T}_{ev}(s)$ is also strictly proper ($\in \mathcal{RH}_2$), provided that

$$\mathbf{D}_a=\mathbf{D}_O\mathbf{D}_{CL}\mathbf{D}_I=0 \tag{A-3}$$

holds, allowing the following definition [14] for its (finite) H_2 norm:

$$\|\mathbf{T}_{ev}\|_2=\left(\frac{1}{2\pi}\int_{-\infty}^{\infty}trace[\mathbf{T}_{ev}^*(j\omega)\mathbf{T}_{ev}(j\omega)]\,d\omega\right)^{1/2} \tag{A-4}$$

Condition (A-3) is quite easily satisfied: considering the definition for $\mathbf{D}_{\mathrm{CL}}$ in (3-II) and substituting $\mathbf{D}_{zd}$ from (5) and $\mathbf{D}_K$=$\mathbf{0}$ for both TMD configurations (see Eqs. (8) and (9)) leads to

$$\mathbf{D}_a=\mathbf{D}_O\mathbf{D}_{\mathrm{CL}}\mathbf{D}_I=\begin{bmatrix}\mathbf{D}_{O,\mathrm{drf}} & \mathbf{0}\\ \mathbf{0} & \mathbf{D}_{O,\mathrm{acc}}\end{bmatrix}\begin{bmatrix}\mathbf{0} & \mathbf{0}\\ \mathbf{0} & \mathbf{M}_s^{-1}\end{bmatrix}\begin{bmatrix}\mathbf{D}_{I,\mathrm{eq}} & \mathbf{0}\\ \mathbf{0} & \mathbf{D}_{I,\mathrm{ext}}\end{bmatrix}=\begin{bmatrix}\mathbf{0} & \mathbf{0}\\ \mathbf{0} & \mathbf{D}_{O,\mathrm{acc}}\mathbf{M}_s^{-1}\mathbf{D}_{I,\mathrm{ext}}\end{bmatrix} \tag{A-5}$$

where we have used a block partitioning of numeric matrices $\mathbf{D}_O$ and $\mathbf{D}_I$ consistent with the partitioning of the transfer matrices W_O and W_I presented in Eqs. (14) and (11), respectively. Eq. (A-5) shows that (A-3) holds iff $\mathbf{D}_{O,\mathrm{acc}}\mathbf{M}_s^{-1}\mathbf{D}_{I,\mathrm{ext}}$ is zero. This means that if the input–output path from external force disturbance to acceleration target output is weighted through an input or output strictly proper filter, (A-3) will be satisfied. Under this condition, the 2-norm is easily computed based on the state-space matrices after solving a Lyapunov equation [14] for which efficient algorithms exist (e.g. see Ref. [46]). The computation of the H_∞ norm (not requiring Eq. (A-3) to be satisfied), on the other hand, is more involved and needs numerical search. Direct application of the formal definition equation (A-2) is not efficient; however, there are other well-established numerical algorithms, e.g. Ref. [47] presents an efficient algorithm (with guaranteed accuracy) based on the relation between the singular values of the transfer function matrix and the eigenvalues of a related Hamiltonian matrix constructed from the state-space matrices of the system.

References

[1] A.K. Agrawal, J.N. Yang, Optimal placement of passive dampers on seismic and wind-excited buildings using combinatorial optimization, *Journal of Intelligent Material Systems and Structures* 10 (1999) 997–1014.

[2] G. Chen, J. Wu, Optimal placement of multiple tune mass dampers for seismic structures, *Journal of Structural Engineering* 127 (9) (2001) 1054–1062.

[3] J.D. Yau, Y.B. Yang, A wideband MTMD system for reducing the dynamic response of continuous truss bridges to moving train loads, *Engineering Structures* 26 (2004) 1795–1807.

[4] A.A. Taflanidis, D.C. Angelides, J.T. Scruggs, Simulation-based robust design of mass dampers for response mitigation of tension leg platforms, *Engineering Structures* 31 (2009) 847–857.

[5] E. Matta, A. De Stefano, Robust design of mass-uncertain rolling-pendulum TMDs for the seismic protection of buildings, *Mechanical Systems and Signal Processing* 23 (2009) 127–147.

[6] L. Petti, M. De Iuliis, Robust design of a single tuned mass damper for controlling torsional response of asymmetric-plan systems, *Journal of Earthquake Engineering* 13 (2009) 108–128.

[7] A. Kareem, S. Kline, Performance of multiple mass dampers under random loading, *Journal of Structural Engineering* 121 (2) (1995) 348–361.

[8] K. Iwanami, K. Seto, Optimum design of dual tuned mass dampers and their effectiveness, *Proceeding of the JSME(C)* 50 (449) (1984) 44–52.

[9] S.-Y. Ok, J. Song, K.-S. Park, Development of optimal design formula for bi-tuned mass dampers using multi-objective optimization, Journal of Sound and Vibration 322 (2009) 60–77. 10.1016/j.jsv.2008.11.023.

[10] C. Li, B. Zhu, Estimating double tuned mass dampers for structures under ground acceleration using a novel optimum criterion, *Journal of Sound and Vibration* 298 (2006) 280–29710.1016/j.jsv.2006.05.018.

[11] R.B. Carneiro, S.M. Avila, J.L.V. De Brito, Parametric study of multiple tuned mass dampers using interconnected masses, *International Journal of Structural Stability and Dynamics* 8 (1) (2008) 187–202.
[12] H. Yamaguchi, N. Harnporchai, Fundamental characteristics of multiple tuned mass dampers for suppressing harmonically forced oscillations, *Earthquake Engineering Structural Dynamics* 22 (1993) 51–62.
[13] L. Zuo, S.A. Nayfeh, Optimization of the individual stiffness and damping parameters in multiple-tuned-mass–damper system, *Journal of Vibration and Acoustics—Transactions of the ASME* 127 (1) (2005) 77–83.
[14] K. Zhou, J.C. Doyle, *Essentials of Robust Control*, Prentice Hall, New Jersey, 1998.
[15] C. Papadimitriou, L.S. Katafygiotis, S.K. Au, Effects of structural uncertainties on TMD design: a reliability-based approach, *Journal of Structural Control* 4 (1) (1997) 65–88.
[16] E. Dehghan-Niri, S.M. Zahrai, A. Mohtat, Effectiveness–robustness objectives in MTMD system design: an evolutionary optimal design methodology, Structural Control and Health Monitoring (2008); 10.1002/stc.297.
[17] A.S. Joshi, R.S. Jangid, Optimum parameters of multiple tuned mass dampers for base-excited damped systems, *Journal of Sound and Vibration* 202 (1997) 657–66710.1006/jsvi.1996.0859.
[18] M.N.S. Hadi, Y. Arfiadi, Optimum design of multi tuned mass damper systems, in: B.H.V. Topping, Z. Bittnar (Eds.), Proceedings of the Sixth International Conference on Computational Structures Technology, Stirling, Scotland, 2002, Paper 42.
[19] S.V. Bakre, R.S. Jangid, Optimum multiple tuned mass dampers for base-excited damped main system, *International Journal of Structural Stability and Dynamics* 4 (4) (2004) 527–542.
[20] L. Zuo, S.A. Nayfeh, Minimax optimization of multi-degree-of-freedom tuned-mass dampers, *Journal of Sound and Vibration* 272 (2004) 893–90810.1016/S0022-460X(03)00500-5.
[21] C.L. Lee, Y.T. Chen, L.L. Chung, Y.P. Wang, Optimal design theories and applications of tuned mass dampers, *Engineering Structures* 28 (2006) 43–53.
[22] M. Abe, Y. Fujino, Dynamic characterization of multiple tuned mass dampers and some design formulas, *Earthquake Engineering and Structural Dynamics* 23 (1994) 813–835.
[23] R. Rana, T.T. Soong, Parametric study and simplified design of tuned mass dampers, *Engineering Structures* 20 (3) (1998) 193–204.
[24] C. Li, Optimum multiple tuned mass dampers for structures under the ground acceleration based on DDMF and ADMF, *Earthquake Engineering and Structural Dynamics* 31 (2002) 897–919.
[25] B. Han, C. Li, Characteristics of linearly distributed parameter-based multiple-tuned mass dampers, *Structural Control and Health Monitoring* 15 (6) (2008) 839–856.
[26] N. Hoang, P. Warnitchai, Design of multiple tuned mass dampers by using a numerical optimizer, *Earthquake Engineering and Structural Dynamics* 34 (2) (2005) 125–144.
[27] H.N. Li, X.L. Ni, Optimization of non-uniformly distributed multiple tuned mass damper, *Journal of Sound and Vibration* 308 (2007) 80–9710.1016/j.jsv.2007.07.014.
[28] E. Dehghan-Niri, A. Mohtat, S.M. Zahrai, Effectiveness-robustness compromise for optimum design of MTMD systems through multi objective GA optimization, *Proceedings of the Seventh European Conference on Structural Dynamics* (*EURODYN 2008*), Southampton, UK, Paper E277.
[29] G.C. Marano, S. Sgobba, R. Greco, M. Mezzina, Robust optimum design of tuned mass dampers devices in random vibrations mitigation, *Journal of Sound and Vibration* 313 (2008) 472–49210.1016/j.jsv.2007.12.020.
[30] A. Packard, G. Balas, R. Liu, J.-Y. Shin, Results on worst-case performance assessment, *Proceedings of the American Control Conference*, Chicago, IL, 2000, pp. 2425–2427.
[31] J. Woodhouse, Linear damping models for structural vibration, *Journal of Sound and Vibration* 215 (3) (1998) 547–56910.1006/jsvi.1998.1709.
[32] J.C. Ramallo, E.A. Johnson, B.F. Spencer Jr., M.K. Sain, Semiactive building base isolation, *American Control Conference*, San Diego, California, June 2–4, 1999.
[33] N. Hoang, Y. Fujino, P. Warnitchai, Optimal tuned mass damper for seismic applications and practical design formulas, *Engineering Structures* 30 (2008) 707–715.
[34] C. Li, Y. Liu, Ground motion dominant frequency effect on the design of multiple tuned mass dampers, *Journal of Earthquake Engineering* 8 (1) (2004) 89–10510.1080/13632460409350482.
[35] C. Li, B. Han, Effect of dominant ground frequency and soil on multiple tuned mass dampers, The Structural Design of Tall and Special Buildings (2009), 10.1002/tal.519.
[36] A. Kareem, S. Kline, Performance of multiple mass dampers under random loading, Technical Report No. 93-004, Department of Civil Engineering and Geological Science, University of Notre Dame, Ind., 1993.
[37] C. Li, B. Han, J. Zhang, Y. Qu, J. Li, Active multiple tuned mass dampers for reduction of undesirable oscillations of structures under wind loads, *International Journal of Structural Stability and Dynamics* 9 (1) (2009) 127–14910.1142/S0219455409002928.
[38] DE. Goldberg, *Genetic Algorithms in Search, Optimization and Machine Learning*, Addison-Wesley, MA, 1989.
[39] X. Du, P.K. Venigella, D. Liu, Robust mechanism synthesis with random and interval variables, *Mechanism and Machine Theory* 44 (7) (2009) 1321–133710.1016/j.mechmachtheory.2008.10.003.
[40] K. Deb, *Multi-Objective Optimization Using Evolutionary Algorithms*, John Wiley & Sons, 2001.
[41] G.J. Balas, A.K. Packard, M.G. Safonov, R.Y. Chiang, Next generation of tools for robust control, *Proceedings of the American Control Conference*, Boston, MA, 2004, pp. 5612–5615.
[42] G. Balas, Synthesis of controllers for the active mass driver system in the presence of uncertainty, *Earthquake Engineering and Structural Dynamics* 27 (1998) 1189–1202.
[43] K. Kanai, Semi-empirical formula for the seismic characteristics of the ground, *Bulletin of the Earthquake Research Institute, The University of Tokyo* 35 (1957) 309–325.
[44] H. Tajimi, A statistical method of determining the maximum response of a building structure during an earthquake, in: *Proceedings of the Second World Conference on Earthquake Engineering*, vol. II, 1960, pp. 781–798.
[45] G. Balas, R. Chiang, A. Packard, M. Safonov, *Robust Control Toolbox™ 3 User's Guide*, The MathWorks, Inc.
[46] R.H. Bartels, G.W. Stewart, Solution of the matrix equation AX+XB=C, *Communications of the ACM* 15 (9) (1972) 820–826.
[47] N.A. Bruisma, M. Steinbuch, A fast algorithm to compute the H_∞-norm of a transfer function matrix, *System Control Letters* 14 (1990) 287–293.